Chem

CellPress

Article

Rapid, multiplexed, and enzyme-free nucleic acid detection using programmable aptamer-based RNA switches

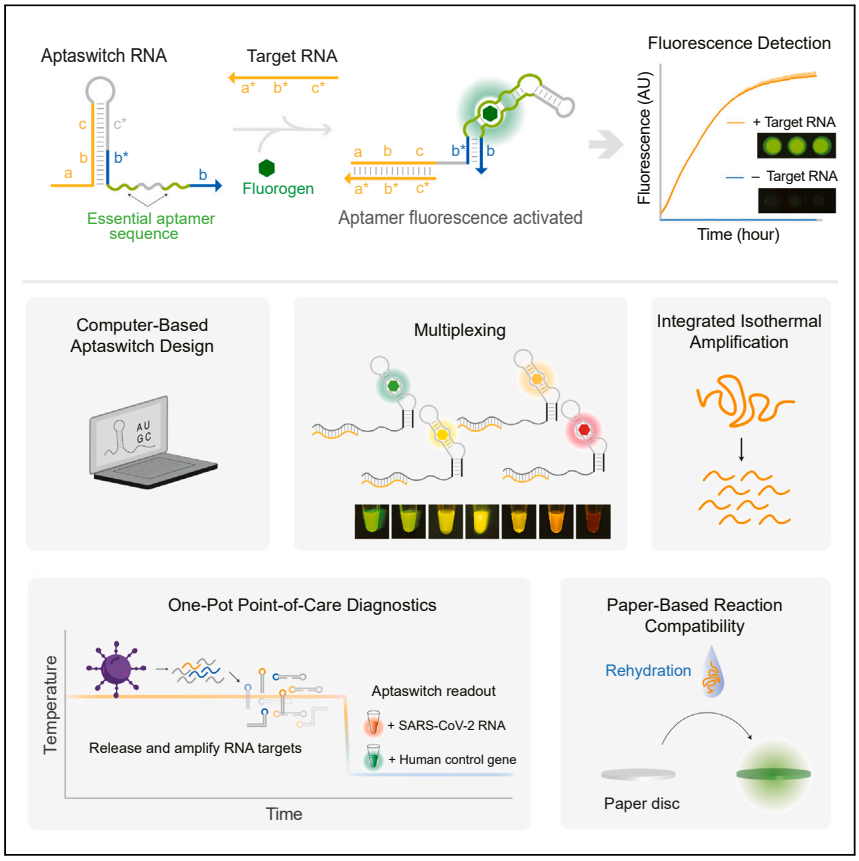

Aptaswitches are programmable nucleic acid sensors that can be interfaced with a rainbow of fluorescent RNA aptamer reporters. These RNA-based switches activate rapidly; provide a strong fluorescent readout; and enable multiplexed, enzyme-free detection of diverse pathogen-related sequences. Aptaswitches can be directly integrated with isothermal amplification to yield all-in-one reactions that detect viruses like SARS-CoV-2 in clinical samples in only 30 min.

Zhaoqing Yan, Amit Eshed, Anli A. Tang, ..., James J. Collins, Peng Yin, Alexander A. Green

aagreen@bu.edu

Highlights

Computer-designed RNA aptaswitches enable rapid detection of target nucleic acids

Aptaswitches provide four-channel multiplexed detection in a single reaction

All-in-one reactions with aptaswitches detect down to attomolar scale in 30 min

All-in-one reactions detect SARS-CoV-2 RNA from clinical samples with 96.67% accuracy

Yan et al., Chem *10*, 1–25
July 11, 2024
https://doi.org/10.1016/j.chempr.2024.03.015

Please cite this article in press as: Yan et al., Rapid, multiplexed, and enzyme-free nucleic acid detection using programmable aptamer-based RNA switches, Chem (2024), https://doi.org/10.1016/j.chempr.2024.03.015

Chem

CellPress

Article

Rapid, multiplexed, and enzyme-free nucleic acid detection using programmable aptamer-based RNA switches

Zhaoqing Yan,[1,2,3] Amit Eshed,[1,3] Anli A. Tang,[4,5] Nery R. Arevalos,[1,3] Zackary M. Ticktin,[4] Soma Chaudhary,[4,5] Duo Ma,[4,5] Griffin McCutcheon,[1,3,4] Yudan Li,[2,3] Kaiyue Wu,[2,3] Sanchari Saha,[4,5] Jonathan Alcantar-Fernandez,[6] Jose L. Moreno-Camacho,[6] Abraham Campos-Romero,[6] James J. Collins,[7,8,9,10] Peng Yin,[9,11] and Alexander A. Green[1,2,3,5,12,*]

SUMMARY

Rapid, simple, and low-cost diagnostic technologies are crucial tools for combating infectious disease. We describe a class of aptamer-based RNA switches, or aptaswitches, that recognize target nucleic acid molecules and initiate the folding of a reporter aptamer. Aptaswitches can detect virtually any sequence and provide an intense fluorescent readout without intervening enzymes, generating signals in as little as 5 min and enabling detection by eye with minimal equipment. Aptaswitches can be used to regulate the folding of seven fluorogenic aptamers, providing a general means of controlling aptamers and an array of multiplexable reporter colors. By coupling isothermal amplification reactions with aptaswitches, we reach sensitivities down to 1 RNA copy/μL in one-pot reactions. Application of multiplexed all-in-one reactions against RNA from clinical saliva samples yields an overall accuracy of 96.67% for detection of SARS-CoV-2 in 30 min. Aptaswitches are thus versatile tools for nucleic acid detection that are readily integrated into rapid diagnostic assays.

INTRODUCTION

Fluorescent light-up aptamers have emerged as powerful tools for visualizing the dynamics of RNA expression in living cells[1–3] and providing a bright, translation-free readout for *in vitro* reactions.[4–6] These systems consist of short sequences of RNA or DNA that bind to conditionally fluorescent dye molecules known as fluorogens to activate their fluorescence. Since the 2003 discovery of the malachite green RNA aptamer,[7] diverse aptamer/fluorogen pairs have been developed with high binding specificity and varying spectral and photophysical properties.[1] In 2014, Filonov et al. reported the Broccoli aptamer that binds to the GFP-mimicking fluorogen (Z)-4-(3,5-difluoro-4-hydroxybenzylidene)-2-methyl-1-(2,2,2-trifluoroethyl)-1H-imidazol-5(4 H)-one (DFHBI-1T) and provides robust folding and green fluorescence in living cells.[8] This work was followed by the development of the Corn, Red Broccoli, and Orange Broccoli aptamers that bind to fluorogens to generate yellow, red/orange, and orange fluorescence, respectively.[9,10] Dolgosheina et al. and Autour et al. have reported the Mango family of aptamers that bind to thiazole orange (TO) derivatives and offer brightness levels that significantly exceed enhanced GFP.[11,12] Chen et al. developed the Pepper aptamer with a broad range of emission maxima with varying (4-((2-hydroxyethyl)(methyl)amino)-benzylidene)-cyanophenylacetonitrile (HBC) analogs spanning from cyan to red.[13,14] These fluorogenic RNA

THE BIGGER PICTURE

Rapid, low-cost, and easy-to-use diagnostics are critical tools for healthcare. By providing accurate disease detection in a convenient format, these tests ensure that patients can receive timely treatment and help slow the spread of infectious diseases. However, implementing such tests for nucleic acids can be challenging without expensive equipment and trade-offs in terms of sensitivity, specificity, and speed. Here, we report a versatile class of sensors termed aptaswitches that manipulate the folding of fluorescent light-up aptamers to enable rapid, low-cost detection of nucleic acid sequences. Aptaswitches operate solely through RNA hybridization and folding, so they do not require enzymes to function and can activate in as little as 5 min. We use them in tandem with isothermal amplification reactions for the detection of viral RNA from clinical samples. These tests provide results within 30 min in an easy-to-deploy format with an accuracy of 96.67% compared to gold-standard tests.

Please cite this article in press as: Yan et al., Rapid, multiplexed, and enzyme-free nucleic acid detection using programmable aptamer-based RNA switches, Chem (2024), https://doi.org/10.1016/j.chempr.2024.03.015

aptamers have been used as tags for *in vivo* mRNA imaging and in biosensors for detecting proteins, small molecules, and nucleic acids.[5,15–19]

Over the last decade, Ebola outbreaks in West Africa, the Zika epidemic, and the COVID-19 pandemic have highlighted the urgent need for rapid, sensitive, and low-cost diagnostics for containing the spread of viruses and ensuring that patients receive timely treatment.[20,21] Nucleic-acid-based biomarkers associated with disease are essential for diagnostics because DNA and RNA can be amplified from trace amounts and provide highly specific detection. Conventional molecular assays, however, are implemented in centralized laboratories with expensive thermal cycling equipment and trained personnel, which increases costs, delays results, and reduces accessibility. These limitations have motivated research into many novel diagnostic technologies.[22–25] To reduce equipment needs, for instance, a variety of nucleic acid amplification methods that take place at a constant temperature have been developed. Unfortunately, these isothermal amplification strategies often suffer from false-positive results arising from non-specific amplification products. Thus, multiple approaches have been developed to verify the sequences of products following isothermal amplification while providing a visible readout. Among the most common are CRISPR-based diagnostic assays.[22] These employ cognate guide RNAs and collateral cleavage to verify the sequence of products and generate visible or fluorescent readout signals.[26–30] Similarly, paper-based cell-free transcription-translation systems have made use of sequence-specific riboregulators to confirm amplicon sequences down to the single-nucleotide level while providing a convenient color-based readout using protein reporters.[21,31–35]

We hypothesized that sequence-specific RNA-based sensors employing fluorescent light-up aptamer reporters could offer compelling advantages over previous sequence-verification methods for diagnostics. For instance, the rainbow of available fluorogenic aptamer colors could offer improved multiplexing capacity and target sequence versatility compared with CRISPR-based methods, which can have protospacer-adjacent motif (PAM) site requirements and more limited multiplexing capacity. Moreover, the rapid folding of aptamers could enable a much faster, enzyme-free readout compared with diagnostics based on cell-free systems, whose readout speed is inherently limited by the rate of translation and protein folding. Although a number of RNA-based sensors using aptamer reporters have been described, which range from split aptamer systems[3,4,36,37] to strand-displacement approaches,[38,39] these systems have been limited in terms of dynamic range, activation speed, sequence versatility, and aptamer compatibility,[3,4,36–41] which has hampered their use in diagnostic applications.

Herein, we report a class of programmable aptamer-based RNA switches, or aptaswitches, that provide wide dynamic range, fast activation speeds, and multiplexing capacity. Aptaswitches do not require enzymes or chemically modified nucleic acids to operate and instead rely on the conditional folding of a fluorogenic reporter aptamer. To do this, they exploit sequence-variable stems identified within the reporter aptamer structure to tightly repress its folding. Upon hybridization with a target nucleic acid sequence, aptaswitches employ a toehold-mediated interaction mechanism to release this repression and promote fast aptamer folding to generate fluorescence, yielding a wide dynamic range up to 260-fold and activation in as little as 5 min. Building on measurements of over a hundred aptaswitches, we implement a computational pipeline for rapid sensor design and demonstrate the generalizability of the aptaswitch mechanism by applying it to five additional fluorogenic aptamer reporters having a variety of fluorescent colors. Coupling the aptaswitches

[1]Department of Biomedical Engineering, Boston University, Boston, MA, USA

[2]Molecular Biology, Cell Biology & Biochemistry Program, Graduate School of Arts and Sciences, Boston University, Boston, MA, USA

[3]Biological Design Center, Boston University, Boston, MA 02215, USA

[4]Biodesign Center for Molecular Design and Biomimetics at the Biodesign Institute, Arizona State University, Tempe, AZ, USA

[5]School of Molecular Sciences, Arizona State University, Tempe, AZ, USA

[6]Innovation and Research Department, Salud Digna, Culiacan, Sinaloa, Mexico

[7]Department of Biological Engineering, Massachusetts Institute of Technology (MIT), Cambridge, MA, USA

[8]Institute for Medical Engineering and Science, MIT, Cambridge, MA, USA

[9]Wyss Institute for Biologically Inspired Engineering, Harvard University, Boston, MA, USA

[10]Broad Institute of MIT and Harvard, Cambridge, MA, USA

[11]Department of Systems Biology, Harvard Medical School, Boston, MA, USA

[12]Lead contact

*Correspondence: aagreen@bu.edu

https://doi.org/10.1016/j.chempr.2024.03.015

Please cite this article in press as: Yan et al., Rapid, multiplexed, and enzyme-free nucleic acid detection using programmable aptamer-based RNA switches, Chem (2024), https://doi.org/10.1016/j.chempr.2024.03.015

with isothermal amplification provides clinically relevant sensitivity with fluorescence that can be seen by eye with minimal equipment. We demonstrate multiplexed all-in-one assays using the aptaswitches that simultaneously detect extracted severe acute respiratory syndrome coronavirus 2 (SARS-CoV-2) RNA and human control transcripts from 60 clinical saliva samples in 30 min with an accuracy of 96.67%. These all-in-one aptaswitch assays are simple to implement and reduce the likelihood of cross-contamination and human error, all while providing highly sensitive detection of viral RNA and human control RNA down to concentrations of 5 and 0.4 copies/μL, respectively. Aptaswitches thus represent powerful enzyme-free molecular sensors for rapid, low-cost, and multiplexed diagnostic assays.

RESULTS

Broccoli aptaswitch design and validation

To implement a programmable aptamer-based switch, we first investigated the Broccoli RNA aptamer, which is known for its robust folding and bright fluorescence upon binding to the fluorogen DFHBI-1T.[8] Reasoning that an aptamer that could tolerate sequence changes would be easier to integrate into such a switch, we examined whether Broccoli could accommodate variations in its stem sequences without abolishing Broccoli/DFHBI-1T fluorescence. Two versions of Broccoli were evaluated: a "standard" version in the same orientation originally reported by Filonov et al.[8] and a "rotated" version formed from a circular permutation of the aptamer that cleaved the aptamer at its apical loop and fused its original 3′ and 5′ ends within a loop (Figure 1A). The base or "stabilizing" stem of these versions of the aptamer, containing the 5′ and 3′ ends of the RNA, was then varied in sequence and tested for fluorescence with DFHBI-1T, while the core Broccoli sequence responsible for ligand binding was kept constant. Encouragingly, we found that both the standard and rotated forms of Broccoli retained strong fluorescence signals for all 14 different stem sequences tested (Figure S1A; Table S1).

With this knowledge, we implemented the first-generation aptaswitch design shown in Figure 1B. Each aptaswitch contains the full sequence of the reporter aptamer, including its core sequence and domains **b** and **b*** encoding the stabilizing stem of the aptamer, where "*" denotes a reverse complementary sequence. In the absence of the target RNA, however, the aptaswitch forces the aptamer into an inactive conformation by sequestering its **b*** stem domain into a strong upstream hairpin structure. The 20-bp hairpin stem is substantially longer than the stabilizing stem, which discourages aptamer folding, and its 5′ positioning ensures that the hairpin can form prior to the aptamer during transcription, further reducing potential leakage. To ensure that the aptaswitches could respond rapidly to diverse target RNAs, we designed them to adopt a toehold-mediated strand-displacement mechanism upon activation to provide fast reaction kinetics[42] (Figure 1B). Thus, each aptaswitch also contains a 15-nt 5′ single-stranded toehold domain **a** that is designed to initiate hybridization with a complementary target RNA. When the target RNA binds, it invades the hairpin stem, disrupting its structure and releasing the aptamer stem domain **b***. To further encourage strand invasion, we incorporated a pair of single-nucleotide bulges into the upper stem of the hairpin in domains **c** and **c′***, with **c** fully complementary to the target RNA, which increased the thermodynamic driving force of the forward reaction[43] and decreased the likelihood of premature transcriptional termination. The stem domain **b*** released from the sequestering hairpin can then hybridize with the exposed **b** domain, promote the folding of the Broccoli reporter aptamer, and generate fluorescence upon binding of DFHBI-1T. Importantly, this general aptaswitch design can be activated by diverse target RNA sequences, provided that the reporter aptamer has a stabilizing stem that can tolerate sequence variations.

Please cite this article in press as: Yan et al., Rapid, multiplexed, and enzyme-free nucleic acid detection using programmable aptamer-based RNA switches, Chem (2024), https://doi.org/10.1016/j.chempr.2024.03.015

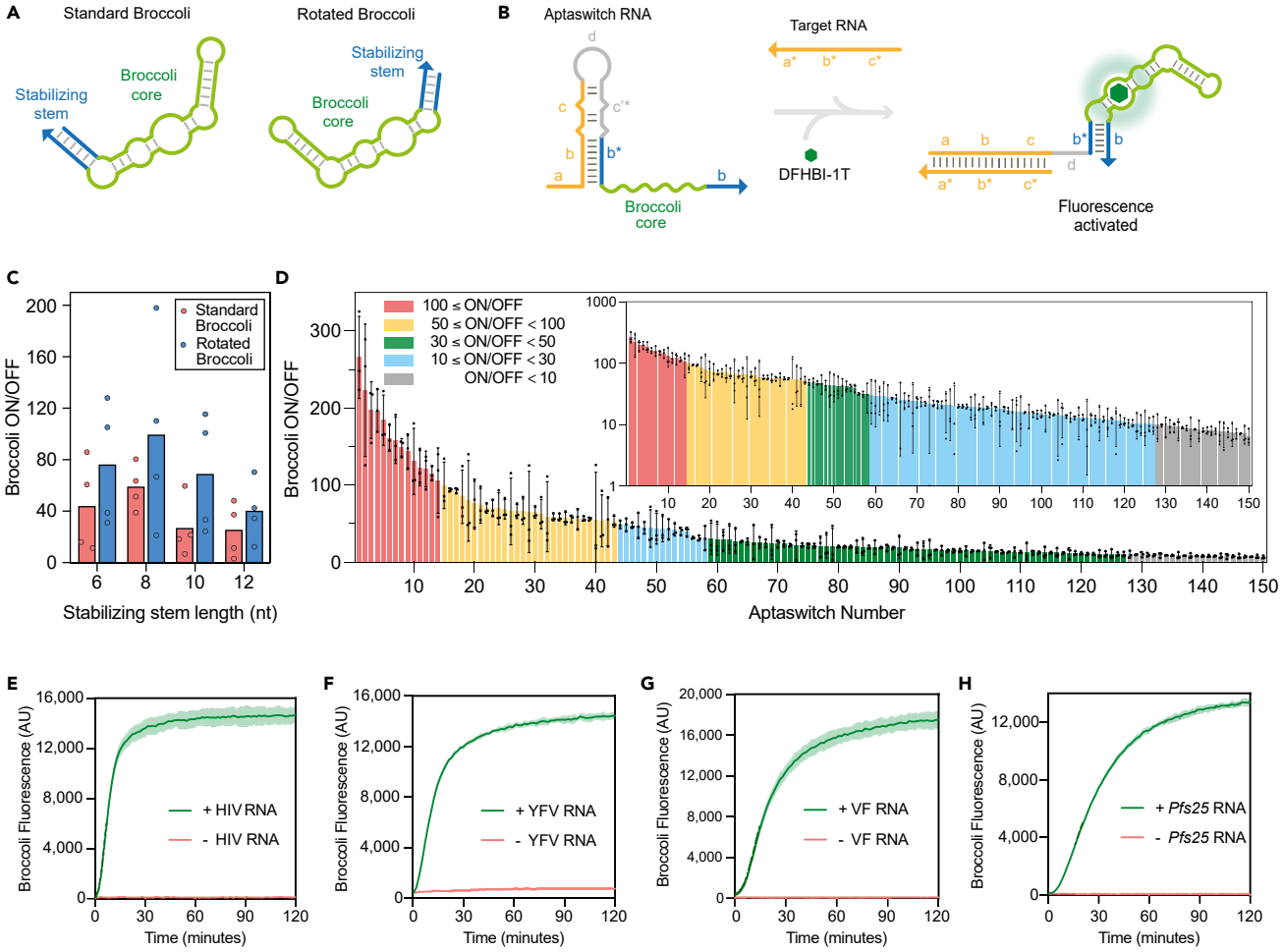

Figure 1. Mechanism of *de novo*-designed aptaswitches and *in vitro* characterization

(A) Structures of the standard and rotated versions of the Broccoli aptamer. Standard Broccoli is the original configuration of Broccoli, and rotated Broccoli is a circularly permuted form of Broccoli.

(B) Design schematics of the Broccoli aptaswitch. Aptaswitches comprise a target-binding sequence that is complementary to a target nucleic acid (shown in orange) and an aptamer core sequence (shown in green). The hairpin structure sequestering the stabilizing stem of Broccoli represses aptamer folding and the formation of the Broccoli/DFHBI-1T complex. The **a*** domain in the target RNA binds to a complementary single-stranded toehold **a** domain in the aptaswitch RNA, initiating a branch migration that opens the hairpin stem. The newly released **b*** domain binds to the downstream **b** domain, enabling the formation of the Broccoli/DFHBI-1T complex.

(C) Evaluation of a library of 32 aptaswitches, with the standard and rotated versions of Broccoli having different stabilizing stem lengths. Data represent mean and individual ON/OFF values after 2 h of four aptaswitch designs with the same stabilizing stem length for each Broccoli version.

(D) ON/OFF fluorescence levels obtained 2 h after reaction for 150 first-generation Broccoli aptaswitches determined in the presence or absence of the cognate target RNAs from different pathogens. Inset: ON/OFF GFP fluorescence measured for Broccoli aptaswitches on a logarithmic scale. Relative errors for the aptaswitch ON/OFF ratios were obtained by adding the relative errors of the aptaswitch ON- and OFF-state fluorescence measurements in quadrature. Relative errors for ON and OFF states are from the SD of $n = 3$ technical replicates.

(E–H) Time course measurements of fluorescence from the top-performing Broccoli aptaswitches for detection of four different pathogens with and without target RNA: HIV (E), YFV (F), VF (G), the malaria-related *Pfs25* transcript (H). Shaded regions denote mean ± SD with $n = 3$ technical replicates.

We used the NUPACK nucleic acid sequence design package[44] to generate initial libraries of *de novo*-designed Broccoli aptaswitches in the standard and rotated configurations with a variety of target RNA sequences (Figure 1C; see Table S1 for sequences). Aptaswitch RNAs were *in vitro* transcribed at 37°C for 2 h with 200 nM of the DNA template and then directly screened for function by challenging them with 2.5 μM synthetic RNA target in 4 μM of DFHBI-1T buffer. The Broccoli aptaswitches routinely achieved greater than 40-fold ON/OFF ratios, which is defined

Please cite this article in press as: Yan et al., Rapid, multiplexed, and enzyme-free nucleic acid detection using programmable aptamer-based RNA switches, Chem (2024), https://doi.org/10.1016/j.chempr.2024.03.015

CellPress

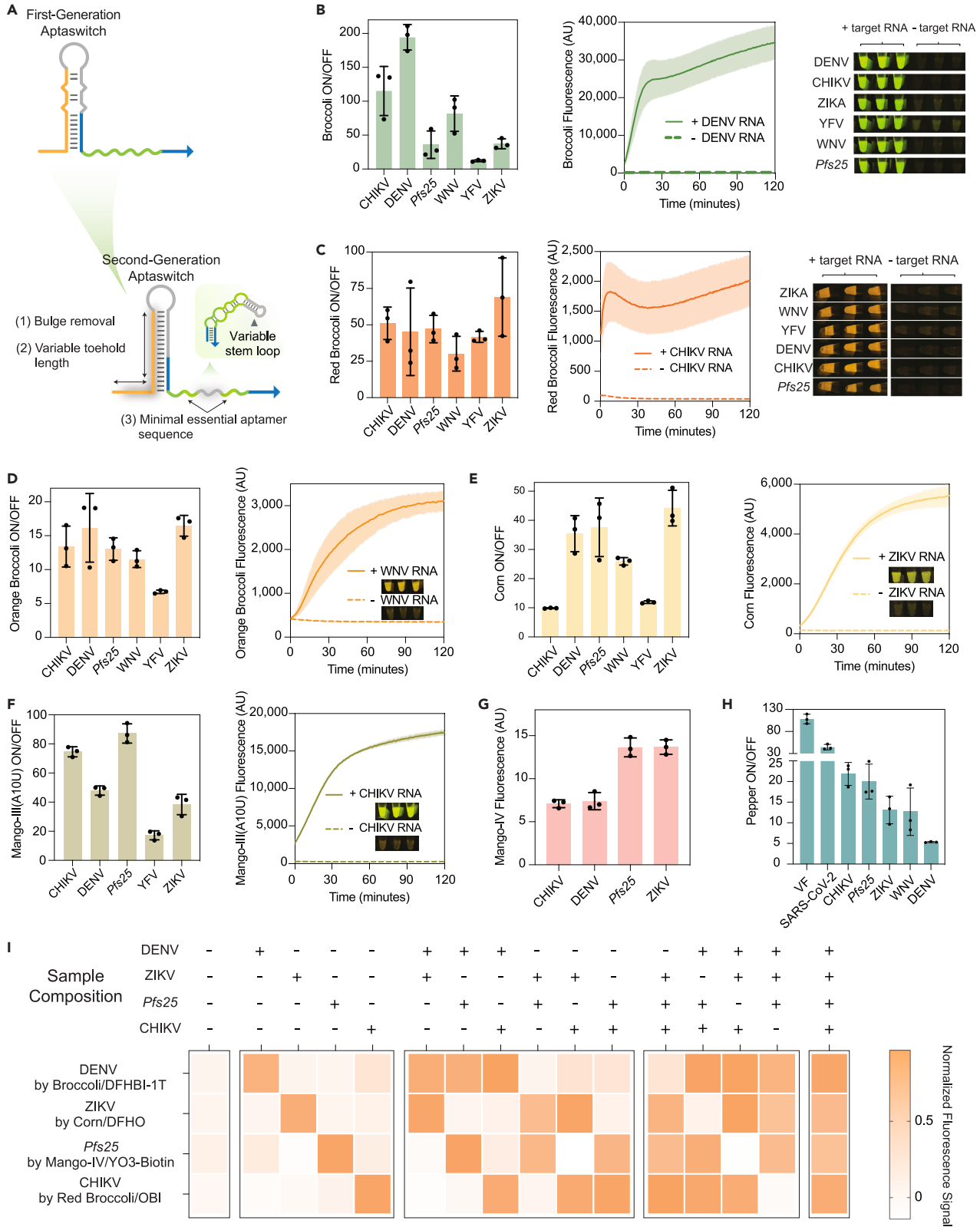

Please cite this article in press as: Yan et al., Rapid, multiplexed, and enzyme-free nucleic acid detection using programmable aptamer-based RNA switches, Chem (2024), https://doi.org/10.1016/j.chempr.2024.03.015

Figure 2. Second-generation aptaswitches enable multiplexed detection with orthogonal reporter aptamers

(A) Schematic of the improved second-generation aptaswitch design compared with the first-generation aptaswitches.

(B and C) ON/OFF fluorescence ratios, time course measurements, and reaction photographs of Broccoli (B) and Red Broccoli (C) aptaswitches.

(D–H) ON/OFF fluorescence ratios and time course measurements of Orange Broccoli (D), Corn (E), Mango-III(A10U) (F), Mango-IV (G), and Pepper (H) aptaswitches. Inset: photographs of aptaswitch reactions.

(I) Multiplexed detection of DENV RNA, ZIKV RNA, *Pfs25* RNA, and CHIKV RNA with Broccoli/DFHBI-1T, Corn/DFHO, Mango-IV/YO3-biotin, and Red Broccoli/OBI, aptamer/fluorogen pairs, respectively. The heatmap represents the arithmetic mean of three replicates.

For (B)–(H), bars represent the arithmetic mean ON/OFF ratio or fluorescence ± SD (n = 3 technical replicates).

as the ratio of the aptaswitch fluorescence with its cognate target divided by the fluorescence of the aptaswitch without it. Moreover, they showed that, on average, the rotated version of Broccoli provided better ON/OFF performance compared with the standard Broccoli. We thus proceeded to evaluate a library of over 150 first-generation aptaswitches using rotated Broccoli targeting a variety of RNAs taken from conserved regions of the genomes of 10 human pathogens: HIV, yellow fever virus (YFV), *Coccidioides* (causative agent of valley fever [VF]), malaria-causing *Plasmodium falciparum* (antigen 25 mRNA, *Pfs25*), dengue virus (DENV), chikungunya virus (CHIKV), St. Louis encephalitis virus (SLEV), West Nile virus (WNV), zika virus (ZIKV), and norovirus (NoV). Candidate Broccoli aptaswitches were designed for each potential binding site along the target RNA in 1-nt increments, leaving flanking regions on the 5′ and 3′ ends of the target available for primer binding. Sensors were designed to target either the sense or antisense orientation of the genome, which can both be readily generated following amplification, and the length of the stabilizing stem domain **b** was varied between 6 and 10 nt. The top six to eight constructs with the lowest overall defects for each target were tested experimentally. Sensor transcripts prepared by *in vitro* transcription were challenged with synthetic versions of the pathogen RNA targets. For determination of the ON/OFF ratio, background fluorescence from the DFHBI-1T fluorogen alone was not subtracted from either the ON- or OFF-state fluorescence.

Figure 1D shows the performance of the top 150 aptaswitches tested based on ON/OFF ratio (see Table S2 for sequences). Overall, we found that 14 aptaswitches from this library provided a remarkable 100-fold or more increase in fluorescence upon detection of the cognate target, and 43 provided a greater than 50-fold ON/OFF ratio. Time course measurements of the optimal Broccoli aptaswitches from four pathogen target RNAs (Figures 1E–1H) demonstrated that the sensors can generate strong fluorescence signals within 15 min in 37°C reactions. The optimal Broccoli aptaswitch for the *P. falciparum* transcript *Pfs25* was also selected for target RNA titration experiments and found to activate with as little as 20 nM of target RNA (Figures S1C and S1D).

Second-generation aptaswitches enable multiplexed detection

To extend the utility of the aptaswitches, we sought to improve their performance using a second-generation design and enable multiplexed readout by integrating other fluorogenic aptamers. Based on the results from the library of first-generation Broccoli aptaswitches, we incorporated three design changes into the second-generation systems (Figures 2A and S2). First, we removed the bulges from the top of the hairpin and set its stem to be 6 bp longer than the stabilizing stem **b** domain of the reporter aptamer. This design change removed the possibility of leakage due to bulges in the stem while reducing the average hairpin length to make it easier to transcribe and disrupt through strand invasion. Second, we allowed the toehold length of the aptaswitches to vary from 10 to 24 nt, depending on the target RNA. Third, for reporter aptamers like Broccoli that have an apical stem loop that tolerates sequence changes, we allowed this stem-loop sequence to be optimized based on

Please cite this article in press as: Yan et al., Rapid, multiplexed, and enzyme-free nucleic acid detection using programmable aptamer-based RNA switches, Chem (2024), https://doi.org/10.1016/j.chempr.2024.03.015

the larger context of the aptaswitch. This sequence was designed to promote the folding of the aptamer, increasing ON-state signal, while minimizing potential for base pairing elsewhere within the aptaswitch, such as in the toehold regions. We then used computational RNA design to generate second-generation aptaswitches using seven different aptamer/fluorogen pairs: Broccoli/DFHBI-1T, Red Broccoli/3,5-difluoro-4-hydroxybenzylidene-imidazolinone-2-oxime-1-benzoimidazole (OBI), Orange Broccoli/3,5-difluoro-4-hydroxybenzylidene imidazolinone-2-oxime (DFHO), Corn/DFHO, Mango-III(A10U)/TO1-biotin, Mango-IV/YO3-biotin, and Pepper/HBC 530. Corn and the Mango aptamers, which lack a variable apical stem loop, were designed with the updated toehold and hairpin alone. With the ongoing concern over mosquito-borne illnesses and the difficulties in identifying them,[21,45–47] we targeted the aptaswitches to conserved genomic regions for these pathogens: CHIKV, DENV, *Pfs25* RNA from *P. falciparum*, WNV, YFV, and ZIKV (see Table S3 for sequences). For the Pepper aptamer, testing was also performed on targets from the fungal infection VF and SARS-CoV-2.

Using the second-generation design, we found that effective aptaswitches could be generated for all seven reporter aptamers for the eight pathogen target RNAs (Figures 2B–2H). The ON/OFF ratios of the aptaswitches varied depending on the target and aptamer, yet they still provided clear differences in signal. Figure S3A presents the ON/OFF ratios for a library of 180 Pepper aptaswitches, providing four sensors with dynamic range greater than 100 and 63 with dynamic range greater than 10. The yield of top-performing aptaswitches was higher for the sensors with rotated versions of Pepper aptamer compared with those with the standard configuration (Figure S3B). Time course measurements of representative aptaswitches from each reporter demonstrated that substantial fluorescence is obtained from the sensors within 30 min, with some generating strong signals within 5–10 min (Figures 2B, 2C, 2F, and S3C). To observe the fluorescence of the aptaswitches, we illuminated the reactions using a blue light transilluminator system equipped with an orange optical filter. The strong fluorescence produced by the aptaswitches with the cognate target was clearly visible using this setup (Figures 2B–2G and S3C). For potential in-home use, we found that inexpensive light and filter combinations costing about $23 could be used to make the aptaswitch reactions visible (Figures S4A–S4C). In addition, we found that the aptaswitch/fluorogen reactions are capable of being lyophilized and reactivated by adding water, suggesting potential for room-temperature storage and distribution (Figure S4D).

The ability to simultaneously detect multiple targets independently is highly desirable, as it can be used to distinguish multiple illnesses that share similar symptoms at higher throughput and lower cost. Taking advantage of the distinct spectral properties of the aptamer/fluorogen pairs, we implemented several multiplexed reactions enabling independent detection of two to three different target RNAs for the mosquito-borne infections (Figures S5A–S5I; see Table S4 for sequences). Leveraging the spectrally orthogonal Broccoli/DFHBI-1T, Corn/DFHO, Mango-IV/YO3-biotin, and Red Broccoli/OBI pairs, we implemented a four-channel reaction for simultaneous detection of targets from DENV, ZIKV, *Pfs25*, and CHIKV, respectively, which could successfully distinguish all 16 possible combinations of targets (Figure 2I; see Figure S5J for photographs of the reactions).

Integrating aptaswitches with isothermal amplification

We next focused on coupling the aptaswitches to isothermal amplification reactions to ensure that they could reach clinically relevant detection limits for pathogen nucleic acids. We first tested the aptaswitches in combination with nucleic acid

Please cite this article in press as: Yan et al., Rapid, multiplexed, and enzyme-free nucleic acid detection using programmable aptamer-based RNA switches, Chem (2024), https://doi.org/10.1016/j.chempr.2024.03.015

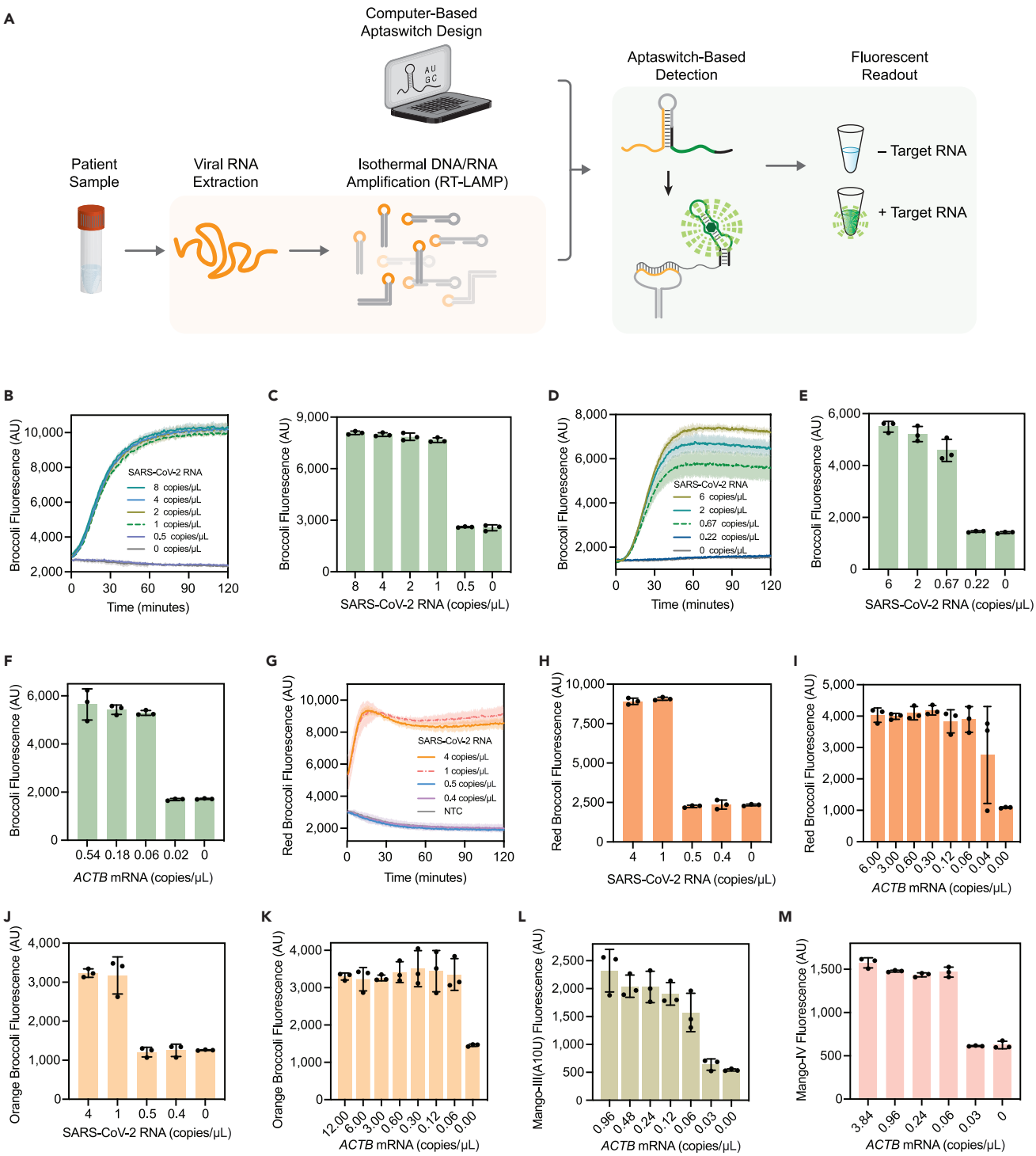

Figure 3. Integration of isothermal amplification with aptaswitches to enable detection of attomolar concentrations of viral RNA

(A) Schematic of the general procedure for the detection of viral RNA. RNA is extracted from patient samples and amplified using RT-LAMP. Amplified nucleic acids are then detected using specific aptaswitches. The aptaswitch binds to exposed loop domains in the RT-LAMP DNA amplicons to produce the output fluorescence signal. A strong fluorescence signal is then used to indicate that viral RNA is present in the patient sample.

(B–F) Representative fluorescence plots of Broccoli aptaswitches for the detection of RT-LAMP amplification for N gene (B) and S gene (D) of RNA from cultured SARS-CoV-2. (C), (E), and (F) show bar graphs of analytical sensitivity determination using series-diluted, cultured SARS-CoV-2 RNA (C and E) or

Please cite this article in press as: Yan et al., Rapid, multiplexed, and enzyme-free nucleic acid detection using programmable aptamer-based RNA switches, Chem (2024), https://doi.org/10.1016/j.chempr.2024.03.015

Figure 3. *Continued*

synthetic human control *ACTB* mRNA (F). Bars in (C), (E), and (F) represent the mean fluorescence intensity ± SD of the aptaswitches at 30 min, which was preceded by a 30-min RT-LAMP reaction.

(G–I) Limit of detection for Red Broccoli aptaswitches for the detection of SARS-CoV-2 N gene (H) and *ACTB* mRNA (I). (G) shows the Red Broccoli aptaswitch response following RT-LAMP with different template concentrations as a function of time (n = 3 technical replicates; bars represent the arithmetic mean ± SD).

(J and K) Limit of detection for Orange Broccoli aptaswitches for the detection of SARS-CoV-2 N gene (J) and human control *ACTB* mRNA (K) (n = 3 technical replicates; bars represent the arithmetic mean ± SD).

(L and M) Fluorescence intensity measured for different human control *ACTB* mRNA concentrations after 30 min of Mango-III(A10U) (L) and Mango-IV aptaswitch (M) (n = 3 technical replicates; bars represent the arithmetic mean ± SD).

sequence-based amplification (NASBA)[48] reactions that operate at 41°C for detection of DENV (Figure S6; see Table S5 for sequences). NASBA followed by aptaswitch readout enabled detection down to sample concentrations of 2.41 RNA copies/μL (Figure S6D) and allowed us to correctly identify three DENV-positive and three DENV-negative serum samples (Figure S6E). However, the 2-h reaction time needed for NASBA reactions prompted us to explore more rapid isothermal amplification methods.

Reverse transcription loop-mediated isothermal amplification (RT-LAMP) is a fast and cost-effective method to amplify specific RNA sequences within minutes.[49,50] RT-LAMP has an operating temperature of ~61°C–71°C and uses a set of four to six primers to generate DNA products containing exposed, single-stranded loop domains.[51,52] We sought to use the aptaswitches in combination with RT-LAMP to develop an assay to detect SARS-CoV-2,[53] which has accounted for more than 670 million infections and more than 6 million deaths worldwide.[49] We thus developed aptaswitches that targeted the exposed loop domains of the RT-LAMP products to activate aptamer fluorescence (Figure 3A). The use of aptaswitches reduces the potential for false-positive results by ensuring that the correct sequence is generated from RT-LAMP, a common failure mode for assays that employ isothermal amplification alone.[22]

We first designed second-generation aptaswitches targeting multiple regions of the SARS-CoV-2 genome and human β-actin (*ACTB*) mRNA, which serves as a sample processing control, using six different reporter aptamers: Broccoli, Red Broccoli, Corn, Mango-III(A10U), Mango-IV, and Orange Broccoli. Initial aptaswitch screens were performed using DNA stem-loop sequences that mimicked the expected RT-LAMP amplicons (see Table S6 for sequences). We observed impressive signal increases greater than 100-fold with rapid system activation against these targets for the Broccoli aptaswitches (Figure S7; see Table S7 for sequences) and the Red Broccoli/OBI aptaswitches (Figures S8A–S8C; see Table S8 for sequences) against SARS-CoV-2 and *ACTB*. Aptaswitches using Corn/DFHO, Mango-III(A10U)/TO1-biotin, Mango-IV/YO3-biotin, and Orange Broccoli/DFHO combinations were also effective at detecting both types of targets, albeit at lower optimal ON/OFF ratios between 20- and 50-fold (Figures S8D–S8N; see Table S8 for sequences).

The top-performing aptaswitches from these screens were coupled to RT-LAMP in two-pot assays using different combinations of primers[50,54–56] and aptaswitches to gauge their sensitivity. In these two-pot reactions, RT-LAMP is first performed on the RNA sample for 30 min at 61°C, and the resulting RT-LAMP product is then diluted into a second reaction at 37°C containing the aptaswitches designed to target the amplicon loop domains. Since RT-LAMP also produces amplicons with two loop regions that have unrelated sequences, we also implemented a scheme to target the two independent loop regions in the same reaction simultaneously

Please cite this article in press as: Yan et al., Rapid, multiplexed, and enzyme-free nucleic acid detection using programmable aptamer-based RNA switches, Chem (2024), https://doi.org/10.1016/j.chempr.2024.03.015

(Figure S9A). This approach effectively doubles the concentration of targets available for detection and thus increases signal output and/or decreases reaction time (Figures S9B–S9D; see Table S9 for sequences). A pair of Broccoli aptaswitches targeting two RT-LAMP loops from amplification of the N gene and S gene provided a limit of detection of 1 copy/μL and 0.67 copies/μL, respectively, in the amplification reaction and activated within 30 min (Figures 3B–3E; see Table S10 for sequences). Using RT-LAMP primers amplifying the human control *ACTB* mRNA and a pair of Broccoli aptaswitches, we achieved an impressive limit of detection of 0.06 copies/μL in the amplification reaction (Figure 3F). Red Broccoli aptaswitches provided red/orange fluorescence, could activate within 15 min, and demonstrated detection limits of 1 and 0.06 copies/μL for the SARS-CoV-2 RNA (N gene) and *ACTB* mRNA, respectively, using the same sets of RT-LAMP primers (Figures 3G–3I). Orange Broccoli, Mango-III(A10U), and Mango-IV were also successfully integrated into the two-pot reaction scheme and provided the same limits of detection as the Broccoli and Red Broccoli sensors (Figures 3J–3M). Experiments performed with these aptamer outputs rapidly provided a visible color that could be seen by the eye using a blue light source and an orange optical filter (Figure S10).

To increase the throughput and ease of implementation of the tests, we also developed master mix formulations for reactions that can be stably stored at −20°C and rapidly added to 384-well plates at the time of use (Figure S11; see Table S11 for sequences). The parallelized two-pot 384-well assay employs a 30-min RT-LAMP reaction, followed by dilution into a 25-min aptaswitch detection reaction. The assay was tested against contrived samples containing extracted RNA from SARS-CoV-2, other human coronaviruses, and influenza at concentrations typical of clinical saliva samples. The high-throughput aptaswitch assay successfully identified the SARS-CoV-2 samples and provided excellent specificity in under 1 h of total reaction time (Figure S11C).

Developing an aptaswitch-based all-in-one molecular diagnostic assay

All-in-one diagnostic assays where all reaction steps occur in the same reaction vessel and do not require additional reagents to be added after the start of the reaction are highly desirable. Such assays reduce processing time, labor, time to result, and the likelihood of cross-contamination while providing increased throughput. Accordingly, we developed a streamlined all-in-one RT-LAMP/aptaswitch assay for detection of SARS-CoV-2 RNA where the reaction is heated 30 min for amplification, followed by a return to room temperature for aptaswitch readout (Figure 4A; see Table S12 for sequences). To implement the assay, we found that it was essential to choreograph binding of the LAMP primers and aptaswitches to the amplicons at different reaction stages to avoid assay inhibition. During the amplification phase, we used a raised 67°C reaction temperature (Figure S12A) and a higher primer/aptaswitch ratio (Figure S12B) to promote primer binding over aptaswitch binding. Once amplification is complete and most of the primers are consumed, the return to room temperature facilitates aptaswitch binding, aptamer folding, and fluorogen docking to generate a strong fluorescence signal (Figures 4A and S12C). We found that standard aptaswitch buffer components and the fluorogen inhibited RT-LAMP reactions (Figure S12D). Thus, we kept the fluorogen concentrations low and did not add additional chemical components to the reactions. We determined that both RT-LAMP and aptaswitch readout worked effectively in these conditions (Figure S12D).

In the optimized all-in-one assays, RNA extracted from a patient sample is added to a reaction combining RT-LAMP components, along with the aptaswitches and

Please cite this article in press as: Yan et al., Rapid, multiplexed, and enzyme-free nucleic acid detection using programmable aptamer-based RNA switches, Chem (2024), https://doi.org/10.1016/j.chempr.2024.03.015

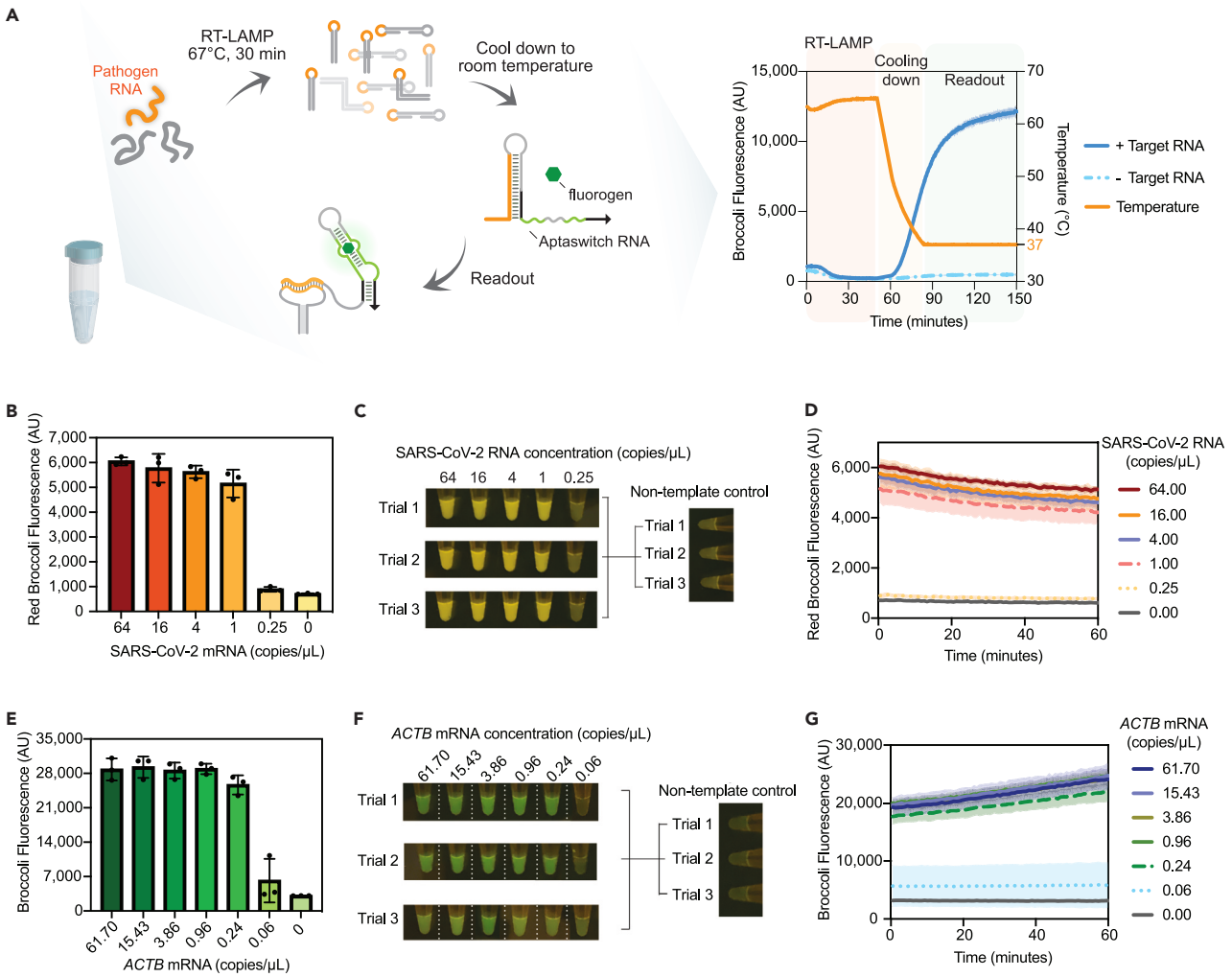

Figure 4. Implementing one-pot single-channel RT-LAMP/aptaswitch reactions

(A) Schematic of target RNA detection by one-pot isothermal amplification-coupled aptaswitch. A 30-min amplification step at 67°C is used for the RT-LAMP reaction and followed by cooling to room temperature. Over this second stage, the reduced temperature enables the aptaswitches to bind to the RT-LAMP amplicons and the cognate fluorogen. A strong and rapid increase in fluorescence is observed in the reaction signaling the presence of target viral RNA.

(B–D) Analytical sensitivity of one-pot Red Broccoli RT-LAMP/aptaswitch reactions for detection of the SARS-CoV-2 N gene using different cultured SARS-CoV-2 RNA template concentrations (B). Photographs (C) from triplicate Red Broccoli aptaswitch reactions following the 30-min amplification at 67°C show strong fluorescence from reactions down to 1 copy/μL. Time course measurements obtained from a plate reader of aptaswitches with different target RNA concentrations at 25°C (D). Bars (B) and shaded regions (D) denote the arithmetic mean ± SD, with $n = 3$ technical replicates.

(E–G) Analytical sensitivity of one-pot Broccoli RT-LAMP/aptaswitch reactions for the detection of human control *ACTB* mRNA at different concentrations (E). Photographs (F) from triplicate Broccoli aptaswitch reactions following the 30-min amplification at 67°C show strong fluorescence from reactions down to 0.24 copies/μL. Time course measurements obtained from a plate reader of aptaswitches with different target RNA concentrations at 25°C (G). Bars (E) and shaded regions (G) denote the arithmetic mean ± SD, with $n = 3$ technical replicates.

fluorogens, for target detection. The reaction vessel is first heated to 67°C for 30 min to amplify the genetic material from the pathogen, followed by cooling to room temperature, where the aptaswitches can bind to the amplicon loops. We first tested reactions using the optimal Red Broccoli aptaswitches targeting SARS-CoV-2. These experiments revealed that the Red Broccoli aptaswitches could provide visible fluorescence output for sample concentrations down to 1 RNA copy/μL in the reaction (Figures 4B and 4C; see Table S13 for sequences). In addition, strong fluorescence was observed from the aptaswitches by the time the system reached room

Please cite this article in press as: Yan et al., Rapid, multiplexed, and enzyme-free nucleic acid detection using programmable aptamer-based RNA switches, Chem (2024), https://doi.org/10.1016/j.chempr.2024.03.015

temperature (Figure 4D). A pair of Broccoli aptaswitches also successfully detected the SARS-CoV-2 S gene in a one-pot single-channel reaction using a temperature-controlled plate reader to provide fluorescence readout in real time (Figure S12E). In addition, we deployed a pair of Broccoli aptaswitches targeting two loops of the RT-LAMP amplicon of the *ACTB* mRNA for detection of the control transcript in a one-pot single-channel reaction (Figures 4E–4G). Once again, Broccoli fluorescence was detectable by the time the reaction reached room temperature (Figures 4F and 4G) and yielded a detection limit of 0.24 copies/μL of *ACTB* mRNA. We also found that the aptaswitch and its cognate fluorogen can be embedded and freeze-dried onto paper discs along with lyophilization-compatible RT-LAMP master mix and primer mix to create a field-stable paper-based one-pot RT-LAMP-coupled aptaswitch assay (Figure S13A). For the diagnostic test, the freeze-dried assay paper is first rehydrated by the solution of extracted RNA and then heated at 67°C for amplification. This step is followed by cooling to room temperature, which enables the proper folding of the aptaswitch and its interaction with the amplicons. A pair of Broccoli aptaswitches successfully detected the SARS-CoV-2 S gene in a paper-based one-pot single-channel reaction. This assay generated green fluorescence emission on paper and employed a temperature-controlled plate reader to provide fluorescence readout in real time (Figures S13B and S13C; see Table S14 for sequences).

We next took advantage of the multiplexing capabilities of the aptaswitches to establish all-in-one RT-LAMP/aptaswitch reactions to detect SARS-CoV-2 and the *ACTB* control mRNA simultaneously (Figure 5A; see Table S15 for sequences). This multiplexed reaction employed 12 different primers from the two sets of RT-LAMP primers, Broccoli and Red Broccoli aptaswitches, and the DFHBI-1T and OBI fluorogens needed for each reporter aptamer. While developing the assay, we found that the Red Broccoli aptaswitches, which favor binding to OBI, also bound to DFHBI-1T in the reaction conditions needed for the all-in-one reactions. This effect led to a strong green fluorescence signal along with the desired red/orange fluorescence upon activation of Red Broccoli. Consequently, we chose to use a Red Broccoli aptaswitch for the detection of SARS-CoV-2 amplicons and a pair of Broccoli aptaswitches for the detection of the *ACTB* amplicon. This combination of sensors still allowed for accurate results to be obtained. Negative clinical samples would generate green fluorescence from the presence of the *ACTB* mRNA in the sample via Broccoli/DFHB-1T, confirming a successful reaction. For samples positive for SARS-CoV-2, a red/orange signal from Red Broccoli/OBI would indicate both the presence of the SARS-CoV-2 amplicon and a successful reaction, obviating the need for readout from the *ACTB* aptaswitch.

We initially tested the multiplexed all-in-one assay using contrived samples with different combinations of the SARS-CoV-2 and *ACTB* synthetic target RNAs and found that it generated the expected two-channel fluorescence signals (Figure 5B). Once the system is activated, the signal remains stable at room temperature over 6 days (Figures S14A and S14B). To assess the sensitivity of the reactions, we prepared synthetic samples with SARS-CoV-2 RNA concentrations varying from 600 to 0.2 copies/μL, while the *ACTB* mRNA concentration was kept constant at 4,000 copies/μL in the reaction (Figure 5C). A significant Red Broccoli fluorescence was observed in the presence of the SARS-CoV-2 N gene down to concentrations of 5 copies/μL, while the assay control green fluorescence remained high for all *ACTB*-containing samples. The assay was then tested by supplying different concentrations of *ACTB* mRNA in the absence of SARS-CoV-2 (Figure 5D). These experiments demonstrated that the all-in-one RT-LAMP/aptaswitch assay could provide significant fluorescence output down to 0.4 RNA copies/μL of the *ACTB* mRNA in the reaction.

Please cite this article in press as: Yan et al., Rapid, multiplexed, and enzyme-free nucleic acid detection using programmable aptamer-based RNA switches, Chem (2024), https://doi.org/10.1016/j.chempr.2024.03.015

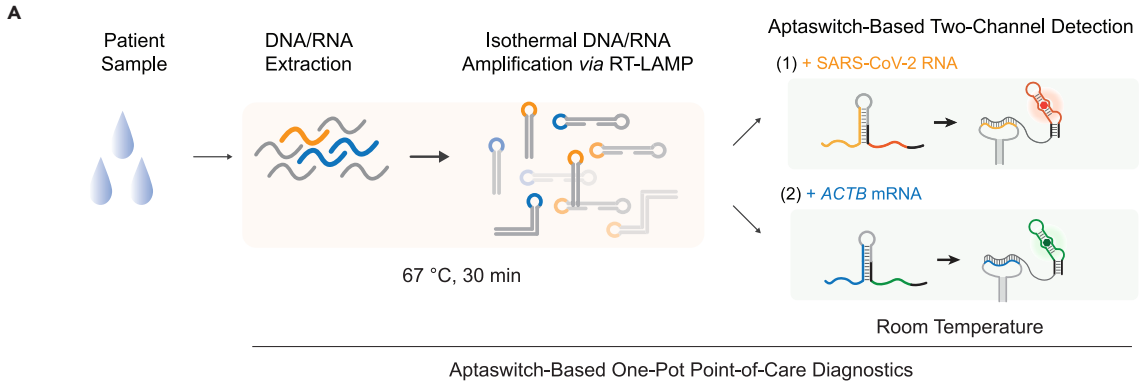

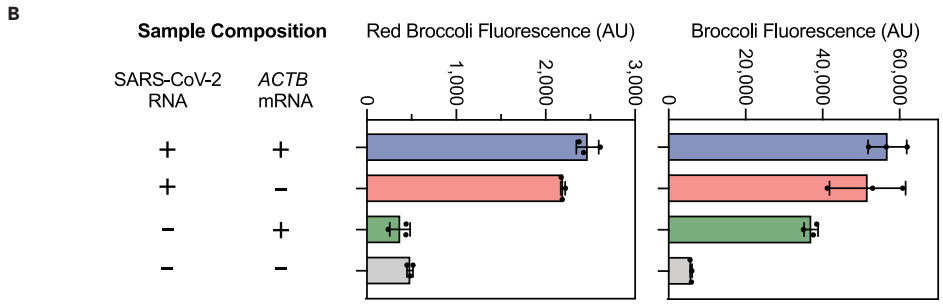

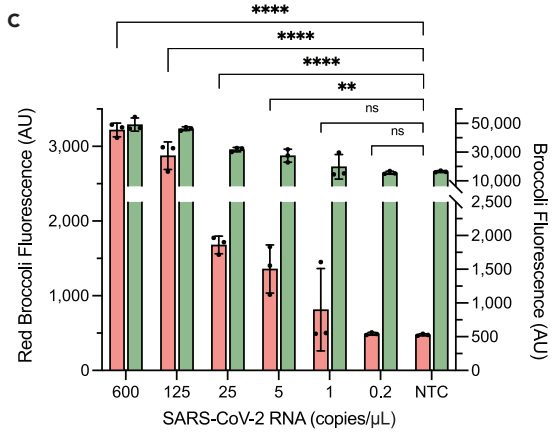

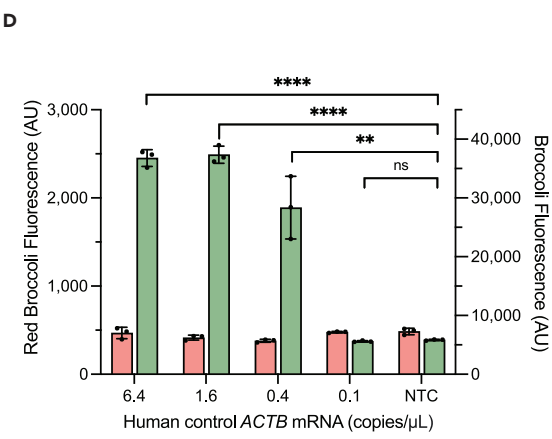

Figure 5. Multiplexed all-in-one RT-LAMP/aptaswitch assay for the detection of viral RNA

(A) Schematic of the multiplexable all-in-one RT-LAMP/aptaswitch assay. RT-LAMP is initially performed at 67°C for 30 min for simultaneous amplification of RNA targets, followed by a cooling period. Reduction of temperature enables binding of the aptaswitches and is evidenced by a rapid increase in the fluorescence of both Broccoli and Red Broccoli aptaswitches, signifying the presence of both the SARS-CoV-2 N gene and the *ACTB* mRNA.

(B) All-in-one reactions enable simultaneous detection of SARS-CoV-2 RNA and human control *ACTB* mRNA with Red Broccoli and Broccoli aptaswitches, respectively (n = 3 technical replicates; bars represent the arithmetic mean ± SD).

(C) Limit of detection assay of SARS-CoV-2 N gene using 4,000 copies/μL *ACTB* mRNA. Values are the arithmetic mean ± SD, with n = 3 technical replicates. Red bar represents fluorescence intensity of Red Broccoli aptaswitches for detecting SARS-CoV-2 RNA. Green bar represents fluorescence intensity of Broccoli aptaswitches for detecting ACTB mRNA (two-tailed Student's t test; ns, $p > 0.05$; ** $p < 0.01$; *** $p < 0.001$; **** $p < 0.0001$).

(D) Limit of detection for multiplexed all-in-one reactions with aptaswitches for *ACTB* mRNA without SARS-CoV-2 RNA (n = 3 technical replicates, two-tailed Student's t test; ns, $p > 0.05$; ** $p < 0.01$; *** $p < 0.001$; **** $p < 0.0001$. Values are the arithmetic mean ± SD. Red bars, fluorescence intensity of Red Broccoli aptaswitches for detecting SARS-CoV-2 RNA; green bars, fluorescence intensity of Broccoli aptaswitches for detecting *ACTB* mRNA).

Please cite this article in press as: Yan et al., Rapid, multiplexed, and enzyme-free nucleic acid detection using programmable aptamer-based RNA switches, Chem (2024), https://doi.org/10.1016/j.chempr.2024.03.015

Validation of multiplexed all-in-one reactions with clinical saliva samples

We next sought to validate the assay using a panel of 31 SARS-CoV-2-positive and 29 negative clinical saliva samples. RNA from the samples was first extracted using a PureLink RNA extraction kit, and SARS-CoV-2 RNA concentrations were quantified via quantitative RT-polymerase chain reaction (RT-qPCR). The extracted RNA was supplied to the reactions and incubated at 67°C for 30 min, followed by rapid cooling for readout in 384-well plates using a plate reader. We used the 95th percentile value for non-template controls (NTC) of 26 valid (*ACTB* mRNA present) and 31 invalid samples (*ACTB* mRNA not present) for threshold value determination of SARS-CoV-2 RNA and human control gene assay channels (Figure S15A). These thresholds from Red Broccoli aptaswitches for determining the presence of SARS-CoV-2 RNA and Broccoli aptaswitches for determining the presence of human control *ACTB* mRNA were then applied to the analysis of data from double-blinded testing of patient saliva samples. Analysis of the samples following reaction cool down enabled immediate identification of positive and negative samples in a plate reader. Figures 6A, 6B, and S15B show the fluorescence of the Red Broccoli and Broccoli aptaswitches at the beginning of the measurement. In general, the SARS-CoV-2 positive samples display a much higher Red Broccoli fluorescence than the negative samples as expected, while the Broccoli fluorescence remains highly active in all the samples. Applying the fluorescence thresholding criteria, the assay identified 29 out of 31 positive samples, which had Ct values ranging from 7 to 30 correctly, while 29 out of 29 negative samples were correctly determined to be free of SARS-CoV-2 RNA. Accordingly, the sensitivity of this assay is 93.55% and the specificity is 100%, resulting in an overall accuracy of 96.67%.

To investigate the potential of the all-in-one assay for rapid high-throughput testing and in-home use, we also evaluated the assay without the RNA extraction step. In this streamlined workflow, the saliva sample is directly added to the RT-LAMP/aptaswitch mixture, and the 67°C reaction temperature is used to simultaneously release viral RNA from the SARS-CoV-2 capsid and amplify its genetic material (Figure 6C). A total of 58 clinical saliva samples were analyzed using this approach (Figures 6D, 6E, and S15C). For the negative patient samples, 29 out of 29 were identified correctly (Figure 6D). However, we found that for positive patient samples with Ct > 24, only 2/10 were identified correctly (Figure 6E). This reduction in sensitivity is likely caused by components from saliva interfering with the RT-LAMP efficiency and less efficient release of viral RNA compared with a full RNA extraction procedure. Despite this limitation, we found that the all-in-one direct-from-saliva assay successfully identified 17 out of 19 positive patient samples with higher viral loads (Ct $\leq$ 24). When considering only these higher viral load saliva samples with Ct $\leq$ 24, the direct assay yielded an accuracy of 95.8%, with 89.5% sensitivity and 100% specificity. Such higher viral load samples are most likely to be obtained in the first days of symptom onset, when samples are known to have lower Ct values.[57] Although the performance of the direct-from-saliva assay is substantially below that of RT-qPCR tests, the ease of implementation and fast 30-min results from these all-in-one tests are advantageous for frequent at-home testing. Moreover, the use of saliva samples, which are collected non-invasively and do not require swabs, makes the direct assay very attractive compared with rapid antigen tests, which typically demonstrate poor sensitivity when used with saliva.[58–60]

DISCUSSION

We have developed a class of computer-designed RNA aptaswitches enabling enzyme-free detection of target nucleic acids without any sequence constraints

Please cite this article in press as: Yan et al., Rapid, multiplexed, and enzyme-free nucleic acid detection using programmable aptamer-based RNA switches, Chem (2024), https://doi.org/10.1016/j.chempr.2024.03.015

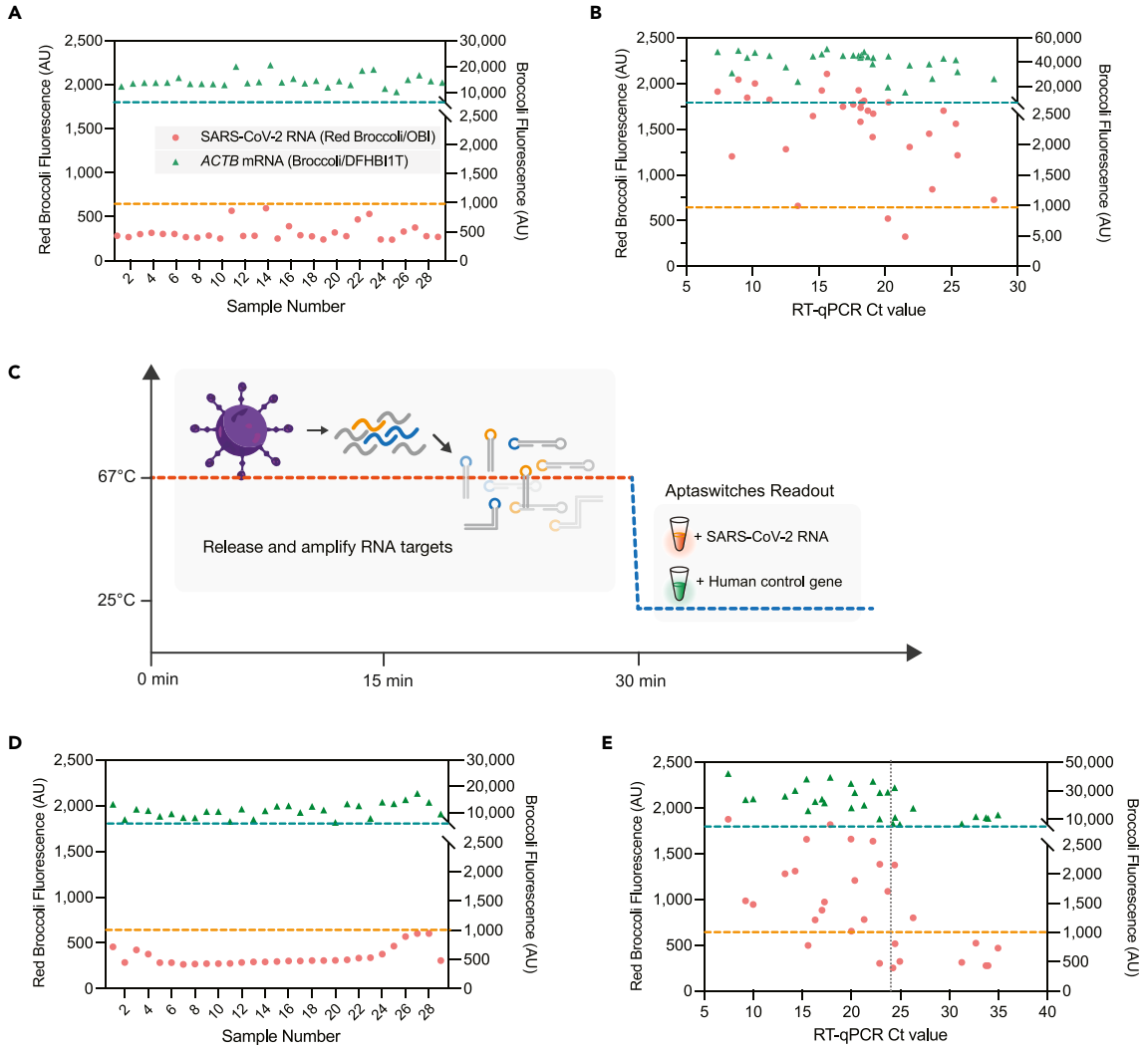

Figure 6. Validation of multiplexed all-in-one RT-LAMP/aptaswitch assays on clinical saliva samples

(A and B) Fluorescence signals obtained from extracted RNA from 29 negative (A) and 31 SARS-CoV-2-positive (B) clinical saliva samples. The dashed lines represent diagnostic thresholds that were determined using 95th percentile values for non-template controls of valid and invalid samples (orange dashed line, Red Broccoli aptaswitch threshold value for determining a SARS-CoV-2-positive sample; teal dashed line, Broccoli aptaswitch threshold value for determining a valid sample based on the presence of the human *ACTB* mRNA).

(C) Schematic of all-in-one extraction-free detection of SARS-CoV-2 RNA in clinical saliva samples. The release of RNA from patient saliva samples occurs at 67°C along with RT-LAMP amplification in the same reaction.

(D and E) Fluorescence signals obtained from extraction-free multiplexed all-in-one RT-LAMP/aptaswitch reactions for 29 negative (D) and 29 (E) positive clinical saliva samples. The dashed lines represent the diagnostic thresholds that were determined using 95th percentile values for non-template controls of SARS-CoV-2-positive and -negative samples (orange dashed line, Red Broccoli aptaswitch threshold value for determining a SARS-CoV-2-positive sample; teal dashed line, Broccoli aptaswitch threshold value for determining a valid sample).

using a variety of different fluorogenic aptamers for readout. Demonstrating the broad adaptability and programmability of this approach, we assembled a set of over 700 aptaswitches capable of targeting diverse RNAs, including pathogens and human transcripts. Taking advantage of spectrally orthogonal aptamer reporters, we implemented a four-channel single-reaction multiplexing detection scheme capable of detecting DENV, ZIKA, malaria, and CHIKV targets simultaneously. This capability can be used to reduce assay costs and processing time. Combining aptaswitches for detection with isothermal reactions for amplification, we achieved clinically relevant levels of sensitivity for viral detection in two-pot

Please cite this article in press as: Yan et al., Rapid, multiplexed, and enzyme-free nucleic acid detection using programmable aptamer-based RNA switches, Chem (2024), https://doi.org/10.1016/j.chempr.2024.03.015

reactions. Use of aptaswitches reduces the potential for false-positive results by ensuring that the correct sequence is generated from isothermal amplification, a common failure mode for assays that employ isothermal amplification alone. We found using RT-LAMP that the sensitivity of the assay is equivalent to RT-qPCR tests conventionally used for SARS-CoV-2 detection in clinical samples. Clear fluorescence signals from the assays can be visualized using simple, readily available components that can be obtained for about $23.

Finally, we also demonstrated all-in-one multiplexed SARS-CoV-2 detection with a human control gene through RT-LAMP/aptaswitch reactions using Red Broccoli/OBI and Broccoli/DFHBI-1T in combination to obtain robust test results within 30 min. This assay was able to reliably detect as few as 5 copies/μL of SARS-CoV-2 with red/orange fluorescence from Red Broccoli while simultaneously providing readout of the assay control *ACTB* mRNA using the Broccoli fluorescence channel. The assay could be extended to higher-order multiplexing with other common respiratory viruses, such as influenza A or respiratory syncytial virus (RSV), using additional orthogonal aptaswitch/fluorogen pairs offering distinct fluorescence signatures.

Key to the high performance and sequence versatility of the aptaswitches is the exploitation of a variable stem region within the reporter aptamers to regulate their folding. Harnessing this feature, which occurred at one or two sites for all fluorogenic aptamers we tested, enabled us to repress or activate aptamer folding using virtually any sequence. The repression mechanism we use based on disruption of the stabilizing stem, in turn, enables the aptaswitches to be activated quickly with high yields since only a single intramolecular hybridization reaction is necessary to form the aptamer. This direct activation mechanism simplifies the design and the aptamer folding pathway compared with other approaches requiring an additional strand-displacement step for activation.[39] The resulting optimized repression and activation mechanisms lead to fast turn-on speed and wide dynamic range, with ON/OFF ratios reaching 260-fold for the best aptaswitches. Furthermore, use of a sequestration mechanism that hides key components of the aptamer, namely the stabilizing stem, within the sensors contributes to the programmability of the aptaswitches. Sequestration means that fewer nucleotides of the aptaswitch are exposed, and only the toehold region of the target-binding site is available for binding, which reduces the likelihood of off-target hybridization and sensor misfolding. By contrast, split aptamer systems, where the reporter aptamer is cleaved in two for repression, employ fully exposed target-binding regions.[3,4,36,37] These exposed regions can lead to sensor misfolding based on the target sequence, hampering recognition of the target molecule and limiting sensor programmability.

Taken together, our all-in-one multiplexed aptaswitch assay is sensitive, low cost, rapid, and easy to use, and it reduces the need for centralized and expensive instrumentation and diagnostic professionals (see Note S1 for comparisons with other diagnostic assays). A key innovative feature of the aptaswitches is their capacity for rapid detection of target nucleic acids in as little as 5 min with a strong characteristic fluorescence signal using a non-enzymatic reaction. This property enhances multiplexing capacity using aptaswitches programmed with distinct fluorescent outputs. Multiplexing of the fluorescence readout, however, is fundamentally limited by the assortment of fluorogenic aptamers available. In principle, increased multiplexing can be achieved by extending aptaswitch designs to aptamers that recognize small molecules or protein ligands, which could enable readout in paper-based

Please cite this article in press as: Yan et al., Rapid, multiplexed, and enzyme-free nucleic acid detection using programmable aptamer-based RNA switches, Chem (2024), https://doi.org/10.1016/j.chempr.2024.03.015

formats rather than via fluorescence. Another advantage of the aptaswitches is that they do not require any chemical modifications for signal generation. As a result, aptaswitches can be prepared simply through *in vitro* transcription at a cost of at most ~$0.21 per reaction, which is substantially lower than the cost of more conventional probe systems using fluorophore-modified oligos[61] (see Note S2 for cost estimate). Although we found that aptaswitch/RT-LAMP reactions can be successfully lyophilized onto paper, for longer-term storage, we expect that they can also be synthesized at the point of use in paper-based reactions using freeze-dried *in vitro* transcription components.[62,63] Lastly, the use of aptaswitches to verify the sequence of amplicons reduces the likelihood of false-positive results from non-specific amplification.[64,65] By contrast, DNA staining dyes, which fluoresce upon binding to DNA irrespective of its sequence, can generate signals from non-specific amplicons, reducing test accuracy.

We anticipate our aptamer-based molecular diagnostic system will enable individuals to on-site test more frequently with a shortened turn-around time,[66,67] particularly when coupled with low-cost instrumentation[68] or microfluidic devices.[30] Compared with widely used rapid antigen tests, our assay provides higher sensitivity and relies on more easily obtained saliva samples, rather than nasal swabs. However, it does demand additional equipment for fluorescence readout, reaction heating at 67°C, and sample purification for optimal performance. Our success in using *in silico* design tools to reliably produce high-performance, specific aptaswitches reduces the number of design cycles required for optimization by improving the components tested with each passing cycle. Thus, multiplexed aptaswitches can also be quickly engineered for profiling custom or newly emerging pathogens. Predicting the performance of the aptaswitches for different targets based on sequence information alone is very challenging and is tied to the large variations in performance observed for different aptaswitch designs (for example, see Figure 1D). These performance differences are driven by multiple effects, including variations in aptamer fluorescence with changes in basal stem sequence (Figure S1A), differences in aptaswitch structure and binding site availability depending on the target sequence, and potential interactions between the target and core aptamer sequence. Despite these effects, we have found that high-performance aptaswitches can be routinely identified through screening six to twelve different sensors for a given target. It is likely that high-throughput aptaswitch datasets coupled with machine learning approaches[69] will enable us to better predict aptaswitch function from sequence in the future. Thermodynamic analyses indicate that the aptaswitch design will be unable to robustly discriminate single-base changes in target sequences (Figure S16; Table S16). However, we expect that future design improvements will enable the use of aptaswitches to resolve such mutations, opening the door to rapid genotyping and variant identification. Furthermore, use of alternative aptamers and substrates should enable the aptaswitches to be used in colorimetric assays that require no additional optical equipment.

The successful integration of aptaswitches with multiple fluorogenic aptamers suggests that they can be broadly applied to diverse aptamers and other functional RNA motifs. Building on the success of toehold-based RNA switches in living cells,[70,71] we expect that aptaswitch mechanisms could be transferred *in vivo* to enable tag-free imaging of endogenous transcripts. These strategies could also be deployed for controlling the folding of functional RNA motifs to regulate intracellular interactions such as protein binding or recognition by the ribosome.[72]

Please cite this article in press as: Yan et al., Rapid, multiplexed, and enzyme-free nucleic acid detection using programmable aptamer-based RNA switches, Chem (2024), https://doi.org/10.1016/j.chempr.2024.03.015

EXPERIMENTAL PROCEDURES

Resource availability

Lead contact

All DNA oligonucleotides were purchased from Integrated DNA Technologies. Further information and requests for resources and reagents should be directed to and will be fulfilled by the lead contact, Alexander A. Green (aagreen@bu.edu).

Materials availability

This study did not generate new, unique reagents.

Data and code availability

The main data supporting the results in this study are available within the paper and the supplemental information. The datasets generated during and/or analyzed during the current study are available from the corresponding authors upon reasonable request.

Transcriptional template preparation and RNA synthesis

All DNA oligonucleotides were purchased from Integrated DNA Technologies (IDT). Molecular biology kits were used as described in the manufacturer's instructions, unless otherwise noted. DNA fragments were assembled and amplified via PCR using the Phusion High-Fidelity (HF) PCR Master Mix with HF buffer (NEB, M0531L). PCR product constituting the transcriptional template for the aptaswitches was purified using a MinElute PCR Purification Kit (Qiagen, 28006).

Aptaswitch RNAs were *in vitro* transcribed at 37°C for 2 h using AmpliScribe T7-Flash Transcription Kits (Biosearch Technologies, ASF3507) with 200 nM of the DNA template. Synthetic target RNAs were synthesized from PCR-amplified templates and were purified using Monarch RNA Cleanup Kit (NEB, T2040L). All transcription products were prepared using this method, unless otherwise noted. For quantification of target RNA concentrations, DNase I (Biosearch Technologies, ASF3507 kit) was used to remove the DNA template to terminate transcription.

In silico design of aptaswitches

Aptaswitches were generated computationally using the NUPACK software package[73,74] and by adapting approaches previously used for designing toehold switch riboregulators.[31,70,75] For a given target RNA or DNA sequence, candidate aptaswitch designs for a desired reporter aptamer were generated at each base along the target RNA or DNA. The secondary structures of the first- and second-generation aptaswitches and the typical ranges of domain lengths are provided in Figure S2. The secondary structures and minimum free energies of each of the resulting aptaswitches were then analyzed in the presence or absence of the target. Candidate aptaswitches were selected based on the predicted single-strandedness of the toehold region, the accessibility of the binding site within the target RNA or DNA, and the probability that the reporter aptamer would fold into the correct secondary structure. This probability was calculated using the equilibrium base-pairing probability table computed for the aptaswitch/target complex. RNA designs, secondary structures, and free energies were computed using NUPACK v3.2.2 using the rna1999 free energy parameter set and a temperature of 37°C.

Experimental screening of aptaswitches

Six to eight promising aptaswitches identified during *in silico* selection were tested for each pathogen target. A BioTek Synergy Neo2 multimode microplate reader was used for all plate reader measurements. 1.0 μM of column-purified aptaswitches (for

Please cite this article in press as: Yan et al., Rapid, multiplexed, and enzyme-free nucleic acid detection using programmable aptamer-based RNA switches, Chem (2024), https://doi.org/10.1016/j.chempr.2024.03.015

Mango-III(A10U) and Mango-IV aptaswitches) or 0.7 μL direct transcription product of aptaswitch RNA (for Broccoli, Corn, Red Broccoli, and Orange Broccoli aptaswitches) and 2.0 μM of purified target RNA were added to the 384-well plate along with 4 μM of DFHBI-1T for Broccoli (Lucerna, 410), 4 μM of BI for Broccoli (Lucerna, 600), 2 μM of DFHO for Corn and Orange Broccoli (Lucerna, 500), 3 μM of OBI for Red Broccoli (Lucerna, 610), 2 μM of TO1-3PEG-biotin for Mango-III(A10U) (abm, G955), 2 μM of YO3-3PEG-biotin for Mango-IV (abm, G957), or HBC 530 for Pepper (tocris, 7277). DFHBI-1T, BI, OBI, TO1-3PEG-biotin, YO1-3PEG-biotin, or HBC 530 buffer consisted of 40 mM HEPES pH 7.4, 100 mM KCl, and 5 mM $MgCl_2$. DFHO buffer consisted of 40 mM HEPES pH 7.4, 100 mM KCl, and 1 mM $MgCl_2$. Before each measurement, samples were shaken linearly for 30 s to ensure proper mixing. The plate reader was preheated, and the measurements were taken at 37°C unless otherwise indicated. To visually observe the fluorescence of the sensors, we illuminated the reactions in a microplate using a Safe Imager 2.0 Blue Light Transilluminator (ThermoFisher, G6600).

Multiplexed detection using orthogonal aptaswitches

Two-channel aptaswitch reactions were prepared with either a 2 μM concentration of the purified Corn aptaswitch or 1.4 μL of the direct transcription product of the Corn aptaswitch along with 1 μM DFHO fluorogen and 1 μM of purified Broccoli aptaswitch or 0.7 μL of the direct transcription product of the Broccoli aptaswitch along with 4 μM of the DFHBI-1T fluorogen. The 10X fluorogenic dye mix consists of 10 μM DFHO, 40 μM DFHBI-1T, 40 mM HEPES pH 7.4, 100 mM KCl, and 5 mM $MgCl_2$.

Three-channel aptaswitch reactions were prepared with 2 μM purified Corn aptaswitch along with 1 μM DFHO, 1 μM purified Broccoli aptaswitch along with 4 μM DFHBI-1T, and 1 μM purified Mango-IV aptaswitch along with 2 μM YO3-biotin. The 10X fluorogenic dye mix consisted of 10 μM DFHO, 40 μM DFHBI-1T, 20 μM YO3-biotin, 40 mM HEPES pH 7.4, 100 mM KCl, and 5 mM $MgCl_2$.

Four-channel aptaswitch reactions were prepared with 2 μM purified Corn aptaswitch along with 1 μM DFHO, 1 μM purified Broccoli aptaswitch along with 4 μM DFHBI-1T, 1 μM purified Mango-IV aptaswitch along with 2 μM YO3-biotin, and 1 μM purified Red Broccoli aptaswitch along with 4 μM DFHBI-1T. The 10X fluorogenic dye mix consisted of 10 μM DFHO, 40 μM DFHBI-1T, 20 μM YO3-biotin, 40 μM OBI, 40 mM HEPES pH 7.4, 100 mM KCl, and 5 mM $MgCl_2$.

Multiplexed reactions were incubated at 37°C for 30 min and transferred to a 384-well plate for fluorescence measurements in a Synergy Neo2 multimode microplate reader. The photographs of fluorescence were taken using a Safe Imager 2.0 Blue Light Transilluminator (Thermo Fisher, G6600).

Analysis of fluorescence data from four-channel multiplexed aptaswitch reactions

Since the fluorescence of the reporter aptamers had some overlap, we implemented a MATLAB script to deconvolve plate reader data and extract the fluorescence generated by each aptamer/fluorogen pair in the four-channel multiplexed reactions. A calibration plate was prepared that contained the aptaswitch reaction buffer with the four fluorogens in one well, representing a blank sample for background fluorescence subtraction, and four other wells containing the fluorogens in buffer with one of the aptamers. The five calibration wells were then measured in a Synergy Neo2 multimode microplate reader using four excitation/emission

Please cite this article in press as: Yan et al., Rapid, multiplexed, and enzyme-free nucleic acid detection using programmable aptamer-based RNA switches, Chem (2024), https://doi.org/10.1016/j.chempr.2024.03.015

pairs: 472 nm/507 nm, 505 nm/545 nm, 595 nm/620 nm, and 541 nm/590 nm. Following subtraction of the background signal, the characteristic profile of the four excitation/emission signals associated with each of the four reporter aptamers was determined, generating a 4 × 4 non-singular matrix linking the fluorescence reads to each aptamer. We inverted this matrix to generate a conversion matrix that could take fluorescence data and convert it into the signal generated by each of the four reporter aptamers. Multiplexed reactions were first measured using identical conditions in the plate reader. Background-subtracted fluorescence from the reactions was then converted into aptamer signals using the conversion matrix (Figure 2I). We also tested the accuracy of the conversion matrix by applying it to all possible combinations of two or more of the aptamers. Comparison of the known aptamer combinations to those generated by the conversion matrix from fluorescence reads yielded an R-squared value of 0.972, confirming the accuracy of the conversion matrix.

NASBA reactions with aptaswitch readout

For target RNA amplification with NASBA, 2.01 μL 3X reaction buffer (Life Sciences, NEC-1-24), 0.99 μL 6X nucleotide mix (Life Sciences, NEC-1-24), 0.03 μL Protector RNase Inhibitor (Roche), 0.12 μL of each NASBA primer (12.5 mM, IDT), 0.15 μL nuclease-free water (Thermo Fisher, 10977015), and 1.2 μL target RNA were mixed at 4°C and heated to 65°C for 2 min, followed by a 10-min incubation at 41°C. 1.5 μL Enzyme Mix (Life Sciences, NEC-1-24) was then added to the reaction for a final volume of 6 μL. After mixing, the reaction was incubated at 41°C for 2 h. For a 35 μL two-pot reaction, 5 μL of the NASBA amplified RNA product was combined with 0.7 μL of RNA aptaswitch and 10X DFHBI-1T dye mix. This reaction was incubated and measured at 37°C for an additional 2 h. The 10X DFHBI-1T dye mix consists of 40 μM DFHBI-1T (Lucerna, 410), 40 mM HEPES (Gibco, 15630080), pH 7.4, 100 mM KCl (Invitrogen, AM9640G), and 5 mM $MgCl_2$ (Invitrogen, AM9530G).

Viral RNA extraction for clinical dengue virus samples

De-identified serum samples positive and negative for dengue virus were obtained at Salud Digna (Culiacan, Mexico). Viral RNA was extracted by using a QIAamp Viral RNA Mini Kit (Qiagen, 52904) according to the manufacturer's instructions. RNA was eluted with 60 μL buffer AVE (Qiagen, 1020953) and stored at −80°C before use.

Two-pot RT-LAMP/aptaswitch reactions

RT-LAMP reactions were conducted with WarmStart LAMP 2X Master Mix (NEB, E1700L), 3 μL of 10X primer mix (IDT; 16 μM of forward inner primer [FIP]/backward inner primer [BIP], 4 μM of forward loop [FLoop]/backward loop [BLoop] primers, and 2 μM of forward outer [F3]/backward outer [B3] primers), and 12 μL of sample. The final volume of the amplification reaction was 30 μL. Amplification was performed at 61°C for 30 min in an Applied Biosystems ProFlex PCR System (Thermo Fisher, 4484073). Heat-inactivated 2019 novel coronavirus (ATCC, VR-1986HK) was used as a template to perform the aptaswitch screen and establish limit of detection ranges. The volume of template to be used and the final concentration of template in the reaction was calculated on the basis of the initial concentration provided by the vendor of 4.2×10^5 copies/μL. 10 μL of the resulting RT-LAMP product was then added to the 384-well plate containing 0.7 μL of directly transcribed aptaswitch RNA (for Broccoli, Corn, Red Broccoli, or Orange Broccoli aptaswitches) along with 4 μM of DFHBI-1T (Lucerna, 410), 2 μM of DFHO (Lucerna, 500), 4 μM of OBI (Lucerna, 610), or 4 μM of DFHO (Lucerna, 500), respectively. For Mango aptaswitches, 1 μM of purified aptaswitch RNA was used with 2 μM of TO1-3PEG-biotin (abm, G955) or 2 μM of YO3-3PEG-biotin (abm, G957).

Please cite this article in press as: Yan et al., Rapid, multiplexed, and enzyme-free nucleic acid detection using programmable aptamer-based RNA switches, Chem (2024), https://doi.org/10.1016/j.chempr.2024.03.015

One-pot single-channel RT-LAMP/aptaswitch reactions

The one-pot single-channel reaction combines RT-LAMP components (WarmStart LAMP 2X Master Mix [NEB, E1700L] and 3 μL 10× primer mix [IDT; 24 μM of FIP/BIP, 6 μM FLoop/BLoop, and 3 μM of F3/B3]) along with the aptaswitches and corresponding fluorogen. These reactions used primers at 1.5× the standard concentrations for RT-LAMP (i.e., 2.4 μM for FIP and BIP, 0.3 μM for F3 and B3, and 0.6 μM for LF and LB primers). For Broccoli aptaswitch readout, the reactions contained 2 μM DFHBI-1T and 0.2 μL of the direct transcription products of each of the Broccoli aptaswitches targeting the forward and backward loops of the SARS-CoV-2 N gene RT-LAMP amplicon. For Red Broccoli readout, the reactions contained 2 μM OBI and 0.4 μL of the direct transcription product of the Red Broccoli aptaswitch targeting the backward loop of the *ACTB* mRNA RT-LAMP amplicon. No additional ions were added. Following addition of the SARS-CoV-2 sample, the reaction was incubated at 67°C for 30 min in a multiwell plate in a temperature-controlled plate reader with the fluorescence readout in real time or incubated in a thermal cycler or incubator. Following the 67°C incubation, the temperature of reaction was cooled to room temperature for aptaswitch binding and fluorescence readout.

Paper-based one-pot single-channel RT-LAMP/aptaswitch reactions

Paper discs (Whatman, 1442-042) were cut using a 7.14 mm hole punch (Amazon, B0879YNTTP) and then pre-treated by blocking overnight in a solution of 5% BSA (NEB, B9000) and 0.05% Tween 20 (Sigma-Aldrich, P1379-100ML), followed by rinsing for 3 × 15 min with H_2O and drying in an oven prior to use. Pre-treated paper discs were then placed into a 96-well flat clear bottom black microplate (Corning, 3603) for freeze-drying and readout reactions. A mix containing 0.2 μL of each directly transcribed aptaswitch RNA, 1.5 μL of 40 μM of DFHBI-1T (Lucerna, 410), 4.5 μM RT-LAMP primer mix (IDT; 16 μM of FIP/BIP, 4 μM FLoop/BLoop, and 2 μM of F3/B3), and 7.5 μL of Lyo-Compatible LAMP 4X Master Mix (NEB, M1710B) was applied to each paper disc (13.9 μL/disc), which was then flash frozen in liquid nitrogen and freeze-dried at −40°C overnight. The stabilized paper reactions were rehydrated with either 30 μL of nuclease-free H_2O or with 30 μL of solution containing target RNA. A BioTek Synergy Neo2 multimode microplate reader was used to control temperature (67°C for 30 or 60 min, following by cooling to 25°C) and monitor fluorescence readout using the excitation/emission pair of 472 nm/507 nm in real time.

All-in-one multiplexed RT-LAMP/aptaswitch reactions

The all-in-one two-channel RT-LAMP/aptaswitch assay was conducted with WarmStart LAMP 2X Master Mix (NEB, E1700L), 3 μL of 10X primer mix, 1.5 μL of 20X fluorogen mix, 0.8 μL of aptaswitch mix, and 9.7 μL of sample. The final volume of the amplification reaction was 30 μL. The 10X RT-LAMP primer mix includes two sets of primers: set 1 for the SARS-CoV-2 N gene at 1.5× the standard RT-LAMP concentration (IDT; 24 μM of FIP/BIP, 6 μM FLoop/BLoop, and 3 μM of F3/B3) and set 2 for the *ACTB* mRNA control at 0.8× the standard RT-LAMP concentration (IDT; 12.8 μM of FIP/BIP, 3.2 μM FLoop/BLoop, and 1.6 μM of F3/B3). The 20X fluorogen mix is composed of 40 μM OBI (Lucerna, 610) and 40 μM DFHBI-1T (Lucerna, 410). No additional ions were added. The aptaswitch mix consists of 2 μL of Broccoli aptaswitch for the *ACTB* mRNA amplicon forward loop, 2 μL of Broccoli aptaswitch for the *ACTB* mRNA amplicon backward loop, and 4 μL of Red Broccoli aptaswitch for the SARS-CoV-2 amplicon backward loop. The reaction was incubated at 67°C for 30 min, followed by a cooling period to 25°C in an Applied Biosystems ProFlex PCR System (Thermo Fisher, 4484073), a temperature-controlled plate reader, or an incubator. The reactions were transferred to a 384-well plate for fluorescence measurements in a Synergy Neo2 multimode microplate reader.

Please cite this article in press as: Yan et al., Rapid, multiplexed, and enzyme-free nucleic acid detection using programmable aptamer-based RNA switches, Chem (2024), https://doi.org/10.1016/j.chempr.2024.03.015

Broccoli/DFHBI-1T fluorescence was measured with 472 nm excitation and 507 nm emission wavelengths. Red Broccoli/OBI fluorescence was measured with 541 nm excitation and 590 nm emission wavelengths.

Viral RNA extraction for clinical SARS-CoV-2 human saliva samples

De-identified, heat-inactivated clinical saliva samples were obtained from the Biodesign Institute Clinical Testing Laboratory at Arizona State University. These specimens were collected for SARS-CoV-2 diagnostic purposes. The viral RNA was extracted, unless otherwise noted, by using a PureLink Viral RNA/DNA Mini Kit (Thermo Fisher, 12280050) according to the manufacturer's instructions. RNA was eluted with 50 μL of H_2O and stored at −80°C before use.

RT-qPCR measurements of clinical samples

RT-qPCR parallel detection was prepared using a Luna SARS-CoV-2 RT-qPCR Multiplex Assay Kit Detection (NEB, E3019). The detection was performed following the protocol of the kit in 7900HT Fast Real-Time PCR System with a 384-well block module (Thermo Fisher, 4329001). Time to threshold was calculated using single-threshold analysis mode.

SUPPLEMENTAL INFORMATION

Supplemental information can be found online at https://doi.org/10.1016/j.chempr.2024.03.015.

ACKNOWLEDGMENTS

We thank the Biodesign Institute Clinical Testing Laboratory at Arizona State University for providing COVID-19-relevant patient samples. We also thank Zhenwei Zhou for helpful discussions on the use of statistical methods for threshold value determination of SARS-CoV-2 diagnostic assays. This work was developed with funding from the Defense Advanced Research Projects Agency (DARPA) (contract no. N66001-23-2-4042); a National Institutes of Health (NIH) Director's New Innovator Award (1DP2GM126892), U01 award (1U01AI148319-01), R01 award (1R01EB031893), and R21 award (1R21AI136571-01A1); a National Science Foundation (NSF) RAPID award (2029532); the Gates Foundation (OPP1160667); Arizona Biomedical Research Centre funds (ADHS16-162400 and CTR051763); an Alfred P. Sloan Fellowship (FG-2017-9108); and Canadian Food Inspection Agency funds (39903-200137) to A.A.G, along with funding from the Salud Digna Research Council (SDI-20166). The views, opinions, and/or findings expressed are those of the authors and should not be interpreted as representing the official views or policies of the Department of Defense or the U.S. Government. The content is solely the responsibility of the authors and does not necessarily represent the official views of the National Institutes of Health.

AUTHOR CONTRIBUTIONS

Z.Y., A.E., A.A.T., N.R.A., Z.M.T., D.M., Y.L., and K.W. performed the experiments. Z.Y. performed most of the wet lab experiments, the design of the sensors and experiments, the selection of viral target sequences, and the analysis of data. Z.Y. conceived and developed second-generation aptaswitch designs; RT-LAMP-coupled, one-pot, and all-in-one multiplexed aptaswitch assays; and the portable home setup for visualizing the signal. Z.M.T., S.C., and S.S. contributed to SARS-CoV-2 patient sample collection. J.A.-F., J.L.M.-C., and A.C.-R. acquired, analyzed, and identified the dengue virus clinical serum samples. A.A.T. designed and performed NASBA-coupled aptaswitch experiments for detecting dengue virus from

patient serum. A.A.G. conceived and conceptualized aptaswitch designs and implemented computer algorithms for aptaswitch design. G.M. optimized the aptaswitch design code and generated aptaswitch designs computationally. Z.Y. and A.A.G. interpreted data and wrote the manuscript. A.A.G., P.Y., and J.J.C. supervised the research.

DECLARATION OF INTERESTS

Z.Y., A.A.T., D.M., and A.A.G. have filed patent applications US20190256898A1 and WO2022046978A3 that describe aspects of this technology. A.A.G. is a cofounder of En Carta Diagnostics Inc. P.Y. is a cofounder, equity holder, director, and consultant of Ultivue, Inc. and Digital Biology, Inc. J.J.C. is a cofounder of Synlogic and Senti Biosciences, a cofounder and director of Sherlock Biosciences, and on the Shape Therapeutics scientific advisory board.

Received: September 14, 2023
Revised: February 2, 2024
Accepted: March 18, 2024
Published: April 12, 2024

REFERENCES

1. Ryckelynck, M. (2020). Development and Applications of Fluorogen/Light-Up RNA Aptamer Pairs for RNA Detection and More. RNA Tagging. Methods Protoc. *2166*, 73–102. https://doi.org/10.1007/978-1-0716-0712-1_5ï.

2. Wang, Q., Xiao, F., Su, H., Liu, H., Xu, J., Tang, H., Qin, S., Fang, Z., Lu, Z., Wu, J., et al. (2022). Inert Pepper aptamer-mediated endogenous mRNA recognition and imaging in living cells. Nucleic Acids Res. *50*, e84. https://doi.org/10.1093/nar/gkac368.

3. Karunanayake Mudiyanselage, A.P.K.K., Yu, Q., Leon-Duque, M.A., Zhao, B., Wu, R., and You, M. (2018). Genetically Encoded Catalytic Hairpin Assembly for Sensitive RNA Imaging in Live Cells. J. Am. Chem. Soc. *140*, 8739–8745. https://doi.org/10.1021/jacs.8b03956.

4. Kolpashchikov, D.M. (2005). Binary malachite green aptamer for fluorescent detection of nucleic acids. J. Am. Chem. Soc. *127*, 12442–12443. https://doi.org/10.1021/ja0529788.

5. Aufdembrink, L.M., Khan, P., Gaut, N.J., Adamala, K.P., and Engelhart, A.E. (2020). Highly specific, multiplexed isothermal pathogen detection with fluorescent aptamer readout. RNA *26*, 1283–1290. https://doi.org/10.1261/rna.075192.120.

6. Jung, J.K., Alam, K.K., Verosloff, M.S., Capdevila, D.A., Desmau, M., Clauer, P.R., Lee, J.W., Nguyen, P.Q., Pastén, P.A., Matiasek, S.J., et al. (2020). Cell-free biosensors for rapid detection of water contaminants. Nat. Biotechnol. *38*, 1451–1459. https://doi.org/10.1038/s41587-020-0571-7.

7. Babendure, J.R., Adams, S.R., and Tsien, R.Y. (2003). Aptamers Switch on Fluorescence of Triphenylmethane Dyes. J. Am. Chem. Soc. *125*, 14716–14717. https://doi.org/10.1021/ja037994o.

8. Filonov, G.S., Moon, J.D., Svensen, N., and Jaffrey, S.R. (2014). Broccoli: rapid selection of an RNA mimic of green fluorescent protein by fluorescence-based selection and directed evolution. J. Am. Chem. Soc. *136*, 16299–16308. https://doi.org/10.1021/ja508478x.

9. Song, W., Filonov, G.S., Kim, H., Hirsch, M., Li, X., Moon, J.D., and Jaffrey, S.R. (2017). Imaging RNA polymerase III transcription using a photostable RNA-fluorophore complex. Nat. Chem. Biol. *13*, 1187–1194. https://doi.org/10.1038/nchembio.2477.

10. Li, X., Mo, L., Litke, J.L., Dey, S.K., Suter, S.R., and Jaffrey, S.R. (2020). Imaging Intracellular S-Adenosyl Methionine Dynamics in Live Mammalian Cells with a Genetically Encoded Red Fluorescent RNA-Based Sensor. J. Am. Chem. Soc. *142*, 14117–14124. https://doi.org/10.1021/jacs.0c02931.

11. Dolgosheina, E.V., Jeng, S.C.Y., Panchapakesan, S.S.S., Cojocaru, R., Chen, P.S.K., Wilson, P.D., Hawkins, N., Wiggins, P.A., and Unrau, P.J. (2014). RNA Mango aptamer-fluorophore: A bright, high-affinity complex for RNA labeling and tracking. ACS Chem. Biol. *9*, 2412–2420. https://doi.org/10.1021/cb500499x.

12. Autour, A., C Y Jeng, S., D Cawte, A., Abdolahzadeh, A., Galli, A., Panchapakesan, S.S.S., Rueda, D., Ryckelynck, M., and Unrau, P.J. (2018). Fluorogenic RNA Mango aptamers for imaging small non-coding RNAs in mammalian cells. Nat. Commun. *9*, 656. https://doi.org/10.1038/s41467-018-02993-8.

13. Chen, X., Zhang, D., Su, N., Bao, B., Xie, X., Zuo, F., Yang, L., Wang, H., Jiang, L., Lin, Q., et al. (2019). Visualizing RNA dynamics in live cells with bright and stable fluorescent RNAs. Nat. Biotechnol. *37*, 1287–1293. https://doi.org/10.1038/s41587-019-0249-1.

14. Huang, K., Chen, X., Li, C., Song, Q., Li, H., Zhu, L., Yang, Y., and Ren, A. (2021). Structure-based investigation of fluorogenic Pepper aptamer. Nat. Chem. Biol. *17*, 1289–1295. https://doi.org/10.1038/s41589-021-00884-6.

15. Urbanek, M.O., Galka-Marciniak, P., Olejniczak, M., and Krzyzosiak, W.J. (2014). RNA imaging in living cells - Methods and applications. RNA Biol. *11*, 1083–1095. https://doi.org/10.4161/rna.35506.

16. Armitage, B.A. (2011). Imaging of RNA in live cells. Curr. Opin. Chem. Biol. *15*, 806–812. https://doi.org/10.1016/j.cbpa.2011.10.006.

17. Zhong, W., and Sczepanski, J.T. (2019). A Mirror Image Fluorogenic Aptamer Sensor for Live-Cell Imaging of MicroRNAs. ACS Sens. *4*, 566–570. https://doi.org/10.1021/acssensors.9b00252.

18. Rogers, T.A., Andrews, G.E., Jaeger, L., and Grabow, W.W. (2015). Fluorescent monitoring of RNA assembly and processing using the split-spinach aptamer. ACS Synth. Biol. *4*, 162–166. https://doi.org/10.1021/sb5000725.

19. You, M., Litke, J.L., Wu, R., and Jaffrey, S.R. (2019). Detection of Low-Abundance Metabolites in Live Cells Using an RNA Integrator. Cell Chem. Biol. *26*, 471–481.e3. https://doi.org/10.1016/j.chembiol.2019.01.005.

20. Khateeb, J., Li, Y., and Zhang, H. (2021). Emerging SARS-CoV-2 variants of concern and potential intervention approaches. Crit. Care *25*, 244. https://doi.org/10.1186/s13054-021-03662-x.

21. Pardee, K., Green, A.A., Takahashi, M.K., Braff, D., Lambert, G., Lee, J.W., Ferrante, T., Ma, D., Donghia, N., Fan, M., et al. (2016). Rapid, Low-Cost Detection of Zika Virus Using Programmable Biomolecular Components. Cell *165*, 1255–1266. https://doi.org/10.1016/j.cell.2016.04.059.

22. Kaminski, M.M., Abudayyeh, O.O., Gootenberg, J.S., Zhang, F., and Collins, J.J. (2021). CRISPR-based diagnostics. Nat. Biomed. Eng. *5*, 643–656. https://doi.org/10.1038/s41551-021-00760-7.

23. Chavda, V.P., Valu, D.D., Parikh, P.K., Tiwari, N., Chhipa, A.S., Shukla, S., Patel, S.S., Balar, P.C., Paiva-Santos, A.C., and Patravale, V. (2023). Conventional and Novel Diagnostic Tools for the Diagnosis of Emerging SARS-CoV-2 Variants. Vaccines *11*, 374. https://doi.org/10.3390/vaccines11020374.

24. Choi, H.K., and Yoon, J. (2023). Nanotechnology-Assisted Biosensors for the Detection of Viral Nucleic Acids: An Overview. Biosensors *13*, 208. https://doi.org/10.3390/bios13020208.

25. Chong, Y.P., Choy, K.W., Doerig, C., and Lim, C.X. (2023). SARS-CoV-2 Testing Strategies in the Diagnosis and Management of COVID-19 Patients in Low-Income Countries: A Scoping Review. Mol. Diagn. Ther. *27*, 303–320. https://doi.org/10.1007/s40291-022-00637-8.

26. Chen, J.S., Ma, E., Harrington, L.B., Da Costa, M., Tian, X., Palefsky, J.M., and Doudna, J.A. (2018). CRISPR-Cas12a target binding unleashes indiscriminate single-stranded DNase activity. Science *360*, 436–439. https://doi.org/10.1126/science.aar6245.

27. Gootenberg, J.S., Abudayyeh, O.O., Lee, J.W., Essletzbichler, P., Dy, A.J., Joung, J., Verdine, V., Donghia, N., Daringer, N.M., Freije, C.A., et al. (2017). Nucleic acid detection with CRISPR-Cas13a/C2c2. Science *356*, 438–442. https://doi.org/10.1126/science.aam9321.

28. Gootenberg, J.S., Abudayyeh, O.O., Kellner, M.J., Joung, J., Collins, J.J., and Zhang, F. (2018). Multiplexed and portable nucleic acid detection platform with Cas13, Cas12a, and Csm6. Science *360*, 439–444. https://doi.org/10.1126/science.aaq0179.

29. Harrington, L.B., Burstein, D., Chen, J.S., Paez-Espino, D., Ma, E., Witte, I.P., Cofsky, J.C., Kyrpides, N.C., Banfield, J.F., and Doudna, J.A. (2018). Programmed DNA destruction by miniature CRISPR-Cas14 enzymes. Science *362*, 839–842. https://doi.org/10.1126/science.aav4294.

30. Chandrasekaran, S.S., Agrawal, S., Fanton, A., Jangid, A.R., Charrez, B., Escajeda, A.M., Son, S., Mcintosh, R., Tran, H., Bhuiya, A., et al. (2022). Rapid detection of SARS-CoV-2 RNA in saliva via Cas13. Nat. Biomed. Eng. *6*, 944–956. https://doi.org/10.1038/s41551-022-00917-y.

31. Ma, D., Shen, L., Wu, K., Diehnelt, C.W., and Green, A.A. (2018). Low-cost detection of norovirus using paper-based cell-free systems and synbody-based viral enrichment. Synth. Biol. (Oxf) *3*, ysy018. https://doi.org/10.1093/synbio/ysy018.

32. Hong, F., Ma, D., Wu, K., Mina, L.A., Luiten, R.C., Liu, Y., Yan, H., and Green, A.A. (2020). Precise and Programmable Detection of Mutations Using Ultraspecific Riboregulators. Cell *180*, 1018–1032.e16. https://doi.org/10.1016/j.cell.2020.02.011.

33. Ma, D., Li, Y., Wu, K., Yan, Z., Tang, A.A., Chaudhary, S., Ticktin, Z.M., Alcantar-Fernandez, J., Moreno-Camacho, J.L., Campos-Romero, A., et al. (2022). Multi-arm RNA junctions encoding molecular logic unconstrained by input sequence for versatile cell-free diagnostics. Nat. Biomed. Eng. *6*, 298–309. https://doi.org/10.1038/s41551-022-00857-7.

34. Karlikow, M., da Silva, S.J.R., Guo, Y., Cicek, S., Krokovsky, L., Homme, P., Xiong, Y., Xu, T., Calderón-Peláez, M.A., Camacho-Ortega, S., et al. (2022). Field validation of the performance of paper-based tests for the detection of the Zika and chikungunya viruses in serum samples. Nat. Biomed. Eng. *6*, 246–256. https://doi.org/10.1038/s41551-022-00850-0.

35. Carr, A.R., Dopp, J.L., Wu, K., Sadat Mousavi, P., Jo, Y.R., McNeley, C.E., Lynch, Z.T., Pardee, K., Green, A.A., and Reuel, N.F. (2022). Toward Mail-in-Sensors for SARS-CoV-2 Detection: Interfacing Gel Switch Resonators with Cell-Free Toehold Switches. ACS Sens. *7*, 806–815. https://doi.org/10.1021/acssensors.1c02450.

36. Torelli, E., Shirt-Ediss, B., Navarro, S.A., Manzano, M., Vizzini, P., and Krasnogor, N. (2023). Light-Up Split Broccoli Aptamer as a Versatile Tool for RNA Assembly Monitoring in Cell-Free TX-TL Systems, Hybrid RNA/DNA Origami Tagging and DNA Biosensing. Int. J. Mol. Sci. *24*, 8483. https://doi.org/10.3390/ijms24108483.

37. Alam, K.K., Tawiah, K.D., Lichte, M.F., Porciani, D., and Burke, D.H. (2017). A Fluorescent Split Aptamer for Visualizing RNA-RNA Assembly in Vivo. ACS Synth. Biol. *6*, 1710–1721. https://doi.org/10.1021/acssynbio.7b00059.

38. Bhadra, S., and Ellington, A.D. (2014). A Spinach molecular beacon triggered by strand displacement. RNA *20*, 1183–1194. https://doi.org/10.1261/rna.045047.114.

39. Wang, T., and Simmel, F.C. (2023). Switchable fluorescent light-up aptamers based on riboswitch architectures. Angew. Chem. Int. Ed. Engl. *62*, e202302858. https://doi.org/10.1002/anie.202302858.

40. Furuhata, Y., Kobayashi, M., Maruyama, R., Sato, Y., Makino, K., Michiue, T., Yui, H., Nishizawa, S., and Yoshimoto, K. (2019). Programmable RNA Detection with a Fluorescent RNA Aptamer Using Optimized Three-way Junction Formation. RNA *25*, 590–599. https://doi.org/10.1261/rna.069062.118.

41. Aw, S.S., Tang, M.X., Teo, Y.N., and Cohen, S.M. (2016). A conformation-induced fluorescence method for microRNA detection. Nucleic Acids Res. *44*, e92. https://doi.org/10.1093/nar/gkw108.

42. Zhang, D.Y., and Winfree, E. (2009). Control of DNA strand displacement kinetics using toehold exchange. J. Am. Chem. Soc. *131*, 17303–17314. https://doi.org/10.1021/ja906987s.

43. Haley, N.E.C., Ouldridge, T.E., Mullor Ruiz, I., Geraldini, A., Louis, A.A., Bath, J., and Turberfield, A.J. (2020). Design of hidden thermodynamic driving for non-equilibrium systems via mismatch elimination during DNA strand displacement. Nat. Commun. *11*, 2562. https://doi.org/10.1038/s41467-020-16353-y.

44. Zadeh, J.N., Steenberg, C.D., Bois, J.S., Wolfe, B.R., Pierce, M.B., Khan, A.R., Dirks, R.M., and Pierce, N.A. (2011). NUPACK: Analysis and design of nucleic acid systems. J. Comput. Chem. *32*, 170–173. https://doi.org/10.1002/jcc.21596.

45. Mordecai, E.A., Caldwell, J.M., Grossman, M.K., Lippi, C.A., Johnson, L.R., Neira, M., Rohr, J.R., Ryan, S.J., Savage, V., Shocket, M.S., et al. (2019). Thermal biology of mosquito-borne disease. Ecol. Lett. *22*, 1690–1708. https://doi.org/10.1111/ele.13335.

46. Lees, R.S., Gilles, J.R., Hendrichs, J., Vreysen, M.J., and Bourtzis, K. (2015). Back to the future: the sterile insect technique against mosquito disease vectors. Curr. Opin. Insect Sci. *10*, 156–162. https://doi.org/10.1016/j.cois.2015.05.011.

47. Caney, S. (2015). Climate change. In The Routledge Handbook of Global Ethics (Routledge), pp. 384–398.

48. Leone, G., Van Schijndel, H., Van Gemen, B., Kramer, F.R., and Schoen, C.D. (1998). Molecular beacon probes combined with amplification by NASBA enable homogeneous, real-time detection of RNA. Nucleic Acids Res. *26*, 2150–2155. https://doi.org/10.1093/nar/26.9.2150.

49. Jiang, M., Pan, W., Aratehfar, A., Fang, W., Ling, L., Fang, H., Daneshnia, F., Yu, J., Liao, W., H.P., et al.. (2020). Development and validation of a rapid, single-step reverse transcriptase loop-mediated isothermal amplification (RT-LAMP) system potentially to be used for reliable and high-throughput screening of COVID-19. Front. Cell. Infect. Microbiol. *10*, 331. https://doi.org/10.1101/2020.03.15.20036376.

50. Zhang, Y., Ren, G., Buss, J., Barry, A.J., Patton, G.C., and Tanner, N.A. (2020). Enhancing Colorimetric LAMP Amplification Speed and Sensitivity with Guanidine Chloride. Biotechniques *69*, 178–185. https://doi.org/10.1101/2020.06.03.132894.

51. Notomi, T., Okayama, H., Masubuchi, H., Yonekawa, T., Watanabe, K., Amino, N., and Hase, T. (2000). Loop-mediated isothermal amplification of DNA. Nucleic Acids Res. *28*, E63. https://doi.org/10.1093/nar/28.12.e63.

52. Zhao, Y., Chen, F., Li, Q., Wang, L., and Fan, C. (2015). Isothermal Amplification of Nucleic Acids. Chem. Rev. *115*, 12491–12545. https://doi.org/10.1021/acs.chemrev.5b00428.

53. Zhou, P., Yang, X.-L., Wang, X.-G., Hu, B., Zhang, L., Si, H.-R., Zhu, Y., Li, B., Huang, C.-L., Chen, H.-D., et al. (2020). Discovery of a novel coronavirus associated with the recent pneumonia outbreak in humans and its potential bat origin. Preprint at bioRxiv. https://doi.org/10.1101/2020.01.22.914952.

54. Huang, W.E., Lim, B., Hsu, C.C., Xiong, D., Wu, W., Yu, Y., Jia, H., Wang, Y., Zeng, Y., Ji, M., et al. (2020). RT-LAMP for rapid diagnosis of coronavirus SARS-CoV-2. Microb. Biotechnol. *13*, 950–961. https://doi.org/10.1111/1751-7915.13586.

55. González-González, E., Lara-Mayorga, I.M., Rodríguez-Sánchez, I.P., Yee-De León, F., García-Rubio, A., Garciaméndez-Mijares, C.E., Guerra-Alvarez, G.E., García-Martínez, G., Aguayo-Hernández, J.A., Márquez-García, E., et al. (2020). Scaling diagnostics in times of COVID-19: colorimetric loop-mediated isothermal amplification (LAMP) assisted by a 3D-printed incubator for cost-effective and scalable detection of SARS-CoV-2. Preprint at medRxiv. https://doi.org/10.1101/2020.04.09.20058651.

56. Buck, M.D., Poirier, E.Z., Cardoso, A., Frederico, B., Canton, J., Barrell, S., Beale, R., Byrne, R., Caidan, S., Crawford, M., et al. (2020). Standard operating procedures for SARS-CoV-2 detection by a clinical diagnostic RT-LAMP assay. Preprint at medRxiv. https://doi.org/10.1101/2020.06.29.20142430.

57. Lin, Y., Wu, P., Tsang, T.K., Wong, J.Y., Lau, E.H.Y., Yang, B., Leung, G.M., and Cowling, B.J. (2023). Viral kinetics of SARS-CoV-2 following onset of COVID-19 in symptomatic patients infected with the ancestral strain and omicron BA.2 in Hong Kong: a retrospective observational study. Lancet Microbe *4*, e722–e731. https://doi.org/10.1016/S2666-5247(23)00146-5.

58. Carreras-Abad, C., To, K.N., Ramkhelawon, L., Planche, T., Monahan, I., Djennad, A., Chalker, V., Heath, P.T., and Le Doare, K. (2021). Detection of group B streptococcus colonisation in pregnant women: Comparison of two different culture methods and study of antimicrobial resistance patterns. J. Infect. *82*, 186–230. https://doi.org/10.1016/j.jinf.2021.01.001.

59. Audigé, A., Böni, J., Schreiber, P.W., Scheier, T., Buonomano, R., Rudiger, A., Braun, D.L., Eich, G., Keller, D.I., Hasse, B., et al. (2021). Reduced relative sensitivity of the elecsys sars-cov-2 antigen assay in saliva compared to nasopharyngeal swabs. Microorganisms *9*, 9. https://doi.org/10.3390/microorganisms9081700.

60. Seitz, T., Schindler, S., Winkelmeyer, P., Zach, B., Wenisch, C., Zoufaly, A., and Allerberger, F. (2021). Evaluation of rapid antigen tests based on saliva for the detection of SARS-CoV-2. J. Med. Virol. *93*, 4161–4162. https://doi.org/10.1002/jmv.26983.

61. Talap, J., Shen, M., Yu, L., Zeng, S., and Cai, S. (2022). RT-LAMP assay combining multi-fluorescent probes for SARS-CoV-2 RNA detection and variant differentiation. Talanta *248*, 123644. https://doi.org/10.1016/j.talanta.2022.123644.

62. Pardee, K., Green, A.A., Ferrante, T., Cameron, D.E., DaleyKeyser, A., Yin, P., and Collins, J.J. (2014). Paper-based synthetic gene networks. Cell *159*, 940–954. https://doi.org/10.1016/j.cell.2014.10.004.

63. Zhang, Y., Zhao, C., Bi, H., Zhang, X., Xue, B., Li, C., Wang, S., Yang, X., Qiu, Z., Wang, J., et al. (2022). A cell-free paper-based biosensor dependent on allosteric transcription factors (aTFs) for on-site detection of harmful metals Hg2+ and Pb2+ in water. J. Hazard. Mater. *438*, 129499. https://doi.org/10.1016/j.jhazmat.2022.129499.

64. Li, B., and Yan, T. (2021). Next generation sequencing reveals limitation of qPCR methods in quantifying emerging antibiotic resistance genes (ARGs) in the environment. Appl. Microbiol. Biotechnol. *105*, 2925–2936. https://doi.org/10.1007/s00253-021-11202-4.

65. Ruiz-Villalba, A., van Pelt-Verkuil, E., Gunst, Q.D., Ruijter, J.M., and van den Hoff, M.J. (2017). Amplification of nonspecific products in quantitative polymerase chain reactions (qPCR). Biomol. Detect. Quantif. *14*, 7–18. https://doi.org/10.1016/j.bdq.2017.10.001.

66. Myhrvold, C., Freije, C.A., Gootenberg, J.S., Abudayyeh, O.O., Metsky, H.C., Durbin, A.F., Kellner, M.J., Tan, A.L., Paul, L.M., Parham, L.A., et al. (2018). Field-deployable viral diagnostics using CRISPR-Cas13. Science *360*, 444–448. https://doi.org/10.1126/science.aas8836.

67. Xia, S., and Chen, X. (2020). Single-copy sensitive, field-deployable, and simultaneous dual-gene detection of SARS-CoV-2 RNA via modified RT–RPA. Cell Discov. *6*, 37. https://doi.org/10.1038/s41421-020-0175-x.

68. De Puig, H., Lee, R.A., Najjar, D., Tan, X., Soeknsen, L.R., Angenent-Mari, N.M., Donghia, N.M., Weckman, N.E., Ory, A., Ng, C.F., et al. (2021). Minimally instrumented SHERLOCK (miSHERLOCK) for CRISPR-based point-of-care diagnosis of SARS-CoV-2 and emerging variants. Sci. Adv. *7*, eabh2944. https://doi.org/10.1126/sciadv.abh2944.

69. Riley, A.T., Robson, J.M., and Green, A.A. (2023). Generative and predictive neural networks for the design of functional RNA molecules. Preprint at bioRxiv. https://doi.org/10.1101/2023.07.14.549043.

70. Green, A.A., Silver, P.A., Collins, J.J., and Yin, P. (2014). Toehold switches: De-novo-designed regulators of gene expression. Cell *159*, 925–939. https://doi.org/10.1016/j.cell.2014.10.002.

71. Kim, J., Zhou, Y., Carlson, P.D., Teichmann, M., Chaudhary, S., Simmel, F.C., Silver, P.A., Collins, J.J., Lucks, J.B., Yin, P., et al. (2019). De novo-designed translation-repressing riboregulators for multi-input cellular logic. Nat. Chem. Biol. *15*, 1173–1182. https://doi.org/10.1038/s41589-019-0388-1.

72. Zhao, E.M., Mao, A.S., de Puig, H., Zhang, K., Tippens, N.D., Tan, X., Ran, F.A., Han, I., Nguyen, P.Q., Chory, E.J., et al. (2022). RNA-responsive elements for eukaryotic translational control. Nat. Biotechnol. *40*, 539–545. https://doi.org/10.1038/s41587-021-01068-2.

73. Zadeh, J.N., Wolfe, B.R., and Pierce, N.A. (2011). Nucleic acid sequence design via efficient ensemble defect optimization. J. Comput. Chem. *32*, 439–452. https://doi.org/10.1002/jcc.21633.

74. Wolfe, B.R., Porubsky, N.J., Zadeh, J.N., Dirks, R.M., and Pierce, N.A. (2017). Constrained Multistate Sequence Design for Nucleic Acid Reaction Pathway Engineering. J. Am. Chem. Soc. *139*, 3134–3144. https://doi.org/10.1021/jacs.6b12693.

75. Wu, K., Yan, Z., and Green, A.A. (2022). Computational Design of RNA Toehold-Mediated Translation Activators. In Riboregulator Design and Analysis (Springer), pp. 33–47. https://doi.org/10.1007/978-1-0716-2421-0_2.